Cement and Concrete Research 156 (2022) 106788

Contents lists available at ScienceDirect

Cement and Concrete Research

journal homepage: www.elsevier.com/locate/cemconres

Influence of aluminum sulfate on properties and hydration of magnesium potassium phosphate cements

Biwan Xu [a,b], Frank Winnefeld [a], Bin Ma [a], Daniel Rentsch [c], Barbara Lothenbach [a,d,*]

[a] Laboratory for Concrete & Asphalt, Swiss Federal Laboratories for Materials Science and Technology (Empa), 8600 Dübendorf, Switzerland
[b] Department of Civil Engineering, Tongji University, 200092 Shanghai, China
[c] Laboratory for Functional Polymers, Swiss Federal Laboratories for Materials Science and Technology (Empa), 8600 Dübendorf, Switzerland
[d] Department of Structural Engineering, Norwegian University of Science and Technology, Trondheim, Norway

ARTICLE INFO

Keywords:
Magnesium potassium phosphate cement
Aluminum sulfate
Compressive strength
Hydration
Thermodynamic modelling

ABSTRACT

Aluminum sulfate shows a positive effect on preventing efflorescence of magnesium potassium phosphate (MKP) cements. Its influence on the MKP cement properties and hydration is explored in this study. Compared to a reference cement (Mg/PO_4 molar ratio = 4, w/c ratio = 0.25), aluminum sulfate retards setting, increases compressive strength, and has little influence on the short-term volume stability. Aluminum sulfate slows down the hydration kinetics, decreases the pH values, accelerates the depletion of KH_2PO_4, and thus mitigates the formation of efflorescence. It also modifies the hydrate assemblage. In addition to K-struvite, aluminum sulfate leads to the formations of arcanite and aluminum-containing hydrates such as amorphous aluminum phosphate, possibly phosphate containing LDH (layered double hydroxide) and minyulite-like phases. The formation of amorphous $MgHPO_4$ and minor amounts of bobierrite and brucite as observed in the reference paste, are suppressed in the presence of aluminum.

1. Introduction

Magnesium potassium phosphate (MKP) cements have a clearly different cement chemistry than Portland cements. They harden through an acid-base reaction between hard- or dead-burnt magnesia (MgO) and potassium monophosphate (KH_2PO_4). The predominant reaction mechanism has been described as follows

$$MgO + KH_2PO_4 + 5H_2O \rightarrow MgKPO_4{\cdot}6H_2O\ (K-struvite) + Heat \quad (1)$$

As represented in Eq. (1), K-struvite is the stoichiometric reaction product of hydrated MKP cements and provides mechanical strength. MKP cements benefit from fast setting, low shrinkage, strong-bonding with pre-existing old Portland cement concrete structures, a near-neutral pH, good immobilization properties for many toxic elements and good biocompatibility [1–12], and thus have many applications, including (but not limited to) construction and rapid repair materials [3], bio-cements [11], and immobilization agents for reactive metals with low-level radioactivity, like metallic aluminum [12,13]. However, a wider application of MKP cements has been hindered mainly by the too fast setting, the significant heat when applied in large structures and by efflorescence which can occur in not well formulated cements [12,14,15].

Efflorescence can also develop on surfaces of Portland cement-based materials; there it contains mainly calcium carbonate, which is aesthetically undesirable but has little impact on material long-term properties and durability [16]. The appearance of efflorescence on MKP cement surfaces, however, is generally associated with potential long-term performance degradation processes such as expansion, strength loss, and low water resistance [14,17,18]. The examination of efflorescence products on MKP cement surfaces showed a mix of unreacted KH_2PO_4 and several intermediate, metastable hydrates such as phosphorrösslerite ($MgHPO_4{\cdot}7H_2O$), $Mg_2KH(PO_4)_2{\cdot}15H_2O$, potassium pyrophosphate ($K_4P_2O_7{\cdot}3H_2O$) and some unidentified phases [17,18]. High magnesium-to-phosphate molar ratios (Mg/PO_4, e.g. >4) and low water-to-binder ratios (w/b, e.g. <0.5) can suppress the occurrence of efflorescence [17,18]. However, high magnesium-to-phosphate molar ratios cause faster cement setting and higher heat release, especially in large cement volumes. Blending MKP cements with mineral additions such as wollastonite, fly ash, or metakaolin could also prevent efflorescence, if the mix designs are optimized [15,19,20]. For

* Corresponding author at: Laboratory for Concrete & Asphalt, Swiss Federal Laboratories for Materials Science and Technology (Empa), 8600 Dübendorf, Switzerland.
E-mail address: Barbara.lothenbach@empa.ch (B. Lothenbach).

https://doi.org/10.1016/j.cemconres.2022.106788
Received 4 January 2022; Received in revised form 21 March 2022; Accepted 22 March 2022
Available online 31 March 2022

Table 1
Chemical composition of the starting materials wt%.

Materials	MgO	SiO_2	Al_2O_3	Fe_2O_3	CaO	K_2O	Na_2O	TiO_2	SO_3	P_2O_5	CO_2[a]	L.O.I.[b]
Magnesia	93.54	4.37	0.04	0.15	1.62	<0.02	<0.04	<0.007	<0.04	0.008	0.18	0.18
KH_2PO_4[c]	0.45	2.01	<0.30	0.07	<0.06	36.63	0.28	0.021	<0.024	40.44	–	20.94

[a] CO_2 content was calculated based on the total carbon content determined by combustion analysis.
[b] Loss on ignition: weight loss recorded upon heating to 950 °C for 60 min.
[c] Oxides and L.O.I. sum up to approx. 101 wt%. This is mainly related to the relative measurement uncertainties of K_2O and P_2O_5 (2.7 wt% and 4.7 wt%, respectively) in the XRF measurement using a pressed powder. The XRF composition indicates a composition of $K_{1.4}H_{1.6}PO_4 1.2H_2O$ instead of KH_2PO_4.

Table 2
Mix designs of the cements used in this study referring to 100 g of magnesia + KH_2PO_4.

Sample	Mg/PO_4 molar ratio[a]	w/c ratio[b]	Magnesia [g]	KH_2PO_4 [g]	$Al_2(SO_4)_3{\cdot}16H_2O$[c]		Water [g]	t_{FS}[d] [min]
					[Al, mM]	[g]		
A: cement paste								
P4-R	4	0.25	54.23	45.77	–	–	25.00	8 ± 1
P4-AlS	4	0.25	54.23	45.77	702	5.53	22.47[b]	17 ± 1
B: cement suspension								
S4-R	4	5	54.23	45.77	–	–	500.00	–
S4-AlS	4	5	54.23	45.77	35	5.53	497.47[b]	–

[a] Based on the chemical compositions of magnesia and KH_2PO_4 given Table 1, the actual Mg/PO_4 molar ratio is 4.9.
[b] w/c = water-to-cement ratio. Cement is referred to the sum of magnesia and KH_2PO_4.
[c] The crystal water of $Al_2(SO_4)_3{\cdot}16H_2O$ was counted as part of the mixing water. It was dissolved in water before use.
[d] t_{FS} = paste final setting time measured by the Vicat needle test using around 200 g fresh paste.

not optimized mixtures, efflorescence together with expansion and cracking could still occur, as reported for fly ash (slag) blended-MKP cements in [14,21].

Aluminum-containing admixtures, e.g. aluminum sulfate, have been used as set accelerators in Portland cements [22]; however, they could behave differently in MKP cements due to the different cement chemistries. Recently aluminum nitrate was reported having a good retardation effect on MKP cement with a Mg/PO_4 molar ratio of 1 and acting more efficiently than boron compounds [6]. The present study not only focuses on the retardation effect of aluminum sulfate, but also on its efflorescence inhibition effect in MKP cement with a high Mg/PO_4 molar ratio of 4 and with the aimed application in the civil engineering field. A series of experiments were carried out on determining the properties and hydration of MKP cements without and with aluminum sulfate; moreover, thermodynamic modelling of the stable hydration products was implemented. For this purpose, a thermodynamic database related to aluminum phosphates was compiled.

2. Materials and methods

2.1. Materials

The starting materials included dead-burnt magnesia (MgO) and KH_2PO_4 in technical grade, and aluminum sulfate ($Al_2(SO_4)_3{\cdot}16H_2O$) in chemical grade. Table 1 gives the chemical compositions of magnesia and KH_2PO_4 as determined by X-ray fluorescence (XRF) analysis. The mineralogical composition of magnesia was determined by X-ray diffraction (XRD, CoKα, PANalytical X'Pert Pro) and has been reported in [2,18,19,23]. The magnesia contained mainly periclase (MgO) and minor amounts of forsterite (Mg_2SiO_4) and monticellite ($CaMgSiO_4$).

Table 2 provides the mix designs of the cement pastes and suspensions investigated in this study. All the cement pastes and suspensions were prepared at the same Mg/PO_4 molar ratio of 4 and at two different w/c ratios of 0.25 and 5. Aluminum sulfate ($Al_2(SO_4)_3{\cdot}16H_2O$) was added to the cements at the same dosages of 5.5%, by weight of magnesia + KH_2PO_4. It was dissolved in water before use, corresponding to the aluminum concentrations of 702 and 35 mM, respectively. It is noted that the letters of 'P', 'R', 'S' and 'AlS' in P4-R, P4-AlS, S4-R and S4-AlS stand for paste, reference, suspension, and aluminum sulfate, respectively; and the number '4' for the Mg/PO_4 molar ratio of 4 used in this study.

2.2. Methods

2.2.1. Compressive strength

Aluminum sulfate ($Al_2(SO_4)_3{\cdot}16H_2O$) was dissolved in water first before adding it to the dry mixture of magnesia and KH_2PO_4 based on the mix designs given in Table 2. The mixing of the pastes was carried out using a vacuum mixer at a speed of 250 rpm for 3 min. Prisms with the dimensions of 20 mm × 20 mm × 100 mm were cast and demoulded right after final setting (see Table 2); afterwards they were cured in air at 20 °C and relative humidity (R.H.) of 70% until the strength test after 7, 28, 217 and 370 days. A three-point bending test was conducted first using a loading rate of 20 N/s and a span of 60 mm. Two prisms were measured for each paste per sample age. Afterwards, the obtained four prim halves were used for compressive strength measurement at a loading rate of 1 MPa/s and a contact surface area of 20 mm × 20 mm.

2.2.2. Volume stability

Following the same casting procedure as described above, prisms with the same dimensions of 20 mm × 20 mm × 100 mm were prepared and demoulded right after final setting (see Table 2). After that, gauge studs were glued to the both ends of each prism sample using an epoxy adhesive. The first length reading was recorded 1 h after the addition of water to the dry cement mixture using a micro-meter comparator (ABOLUTE, Mitutoyo). All prisms were stored in a curing room at 20 °C and a R.H. of 70%. The prism lengths were measured periodically to obtain the relative length changes over time. Triplicated prisms were measured for each mix.

2.2.3. Isothermal calorimetry

Hydration heat of the pastes was determined using an isothermal conduction calorimeter (TA instruments, TAM Air, equipped with Admix ampoules) at 20 °C. As given in Table 2, magnesia and KH_2PO_4 were weighted into ampoules and dry-mixed first. Aluminum sulfate ($Al_2(SO_4)_3{\cdot}16H_2O$) was dissolved in deionized water before use. The deionized water or aluminum sulfate solution was kept in syringes inside the calorimeter, and was injected into the ampoules once the

Table 3
Stability constants and solubility products (log K_{so}^{o}) of aluminum and phosphate containing aqueous complexes and solids at 25 °C and 1 bar added to the Cemdata18 [32], and the magnesium calcium phosphate database [19,23,33].

Species	Reaction	log K_{so}^{o}	$\Delta_f G^{\circ}$ (kJ/mol)	Reference
Aqueous species				
$Al(H_2PO_4)_2^{+}$	$Al^{3+} + 4H^{+} + 2PO_4^{-3} \Leftrightarrow AlH_4(PO_4)_2^{+2}$	45.50	−2780.72	[34,35]
$AlH_2PO_4^{+2}$	$Al^{3+} + 2H^{+} + PO_4^{-3} \Leftrightarrow AlH_2PO_4^{+2}$	22.2	−1629.07	[34]
$AlHPO_4^{+}$	$Al^{3+} + H^{+} + PO_4^{-3} \Leftrightarrow AlHPO_4^{+}$	21.6	−1625.65	[35]
$AlPO_4^{0}$	$Al^{3+} + PO_4^{-3} \Leftrightarrow AlPO_4^{0}$	20.5	−1619.37	[35]

Solids	Reaction	Volume (cm^3/mol)	log K_{so}^{o}	$\Delta_f G$ (kJ/mol)	Reference*
Solids					
Berlinite:	$AlPO_4 \Leftrightarrow Al^{3+} + PO_4^{3-} + 2H_2O$	46.58	−20.24	−1617.9	[39,40]
Variscite:	$AlPO_4{\cdot}2H_2O \Leftrightarrow Al^{3+} + PO_4^{3-} + 2H_2O$	60.96	−25.1[a]	−2120.0	ts, [41]
Amorphous aluminum phosphate:	$AlPO_4{\cdot}2H_2O \Leftrightarrow Al^{3+} + PO_4^{3-} + 2H_2O$	60.96	−23.7[b]	2112.0	ts
Augellite:	$Al_2(PO_4)(OH)_3 + 3H^{+} \Leftrightarrow 2Al^{3+} + PO_4^{3-} + 3H_2O$	73.89	−19.71	−2810.1	[42,43]
Senegalite:	$Al_2(PO_4)(OH)_3{\cdot}H_2O + 3H^{+} \Leftrightarrow 2Al^{3+} + PO_4^{3-} + 4H_2O$				
(Estimated log K_{so}^{o} and $\Delta_f G^{\circ}$ values)		85.67	*−19.71*	*−3047.3*[c]	ts, [44]
Wavellite:	$Al_3(PO_4)_2(OH)_3{\cdot}5H_2O + 3H^{+} \Leftrightarrow 3Al^{3+} + 2PO_4^{3-} + 8H_2O$	175.9	−31.33	−5564.7	[45,46]
Trolleite:	$Al_4(PO_4)_3(OH)_3 + 3H^{+} \Leftrightarrow 4Al^{3+} + 3PO_4^{3-} + 3H_2O$	143.7	−65.72	−6077.5	[42,47]
Taranakite:	$K_3Al_5(HPO_4)_6(PO_4)_2{\cdot}18H_2O \Leftrightarrow 3\,K^{+} + 6H^{+} + 5Al^{3+} + 8PO_4^{3-} + 18H_2O$	625.7	−190.1[d]	−16,769.5[d]	ts, [48]
Basic potassium aluminate phosphate (minyulite type):	$KAl_2(PO_4)_2OH{\cdot}2H_2O + H^{+} \Leftrightarrow K^{+} + 2Al^{3+} + 2PO_4^{3-} + 3H_2O$	132.2	−46.3[e]	−4263.0[e]	ts, [49]
Layered double hydroxides (LDH):	$OH\text{-}LDH{:}Mg_4Al_2(OH)_{14}{\cdot}3H_2O \Leftrightarrow 4Mg^{2+} + 2Al(OH)_4^{-} + 6OH^{-} + 3H_2O$	220	−56.0	−6394.6	[32]
PO_4-LDH:	$Mg_4Al_2(OH)_{12}(HPO_4)_2{\cdot}4H_2O \Leftrightarrow 4Mg^{2+} + 2Al(OH)_4^{-} + 4OH^{-} + HPO_4^{2-} + 4H_2O$				
(Estimated volumes, log K_{so}^{o}, $\Delta_f G^{\circ}$ values)		*222*	*−53.0*	*−7389.1*	ts, [50]
PO_4-LDH:	$Mg_6Al_2(OH)_{16}(HPO_4)_2{\cdot}5H_2O \Leftrightarrow 6Mg^{2+} + 2Al(OH)_4^{-} + 8OH^{-} + HPO_4^{2-} + 5H_2O$				
(Estimated volumes, log K_{so}^{o}, $\Delta_f G^{\circ}$ values)		*301*	*−75.3*	*−9290.6*	ts, [50]
PO_4-LDH:	$Mg_8Al_2(OH)_{20}(HPO_4)_2{\cdot}6H_2O \Leftrightarrow 8Mg^{2+} + 2Al(OH)_4^{-} + 12OH^{-} + HPO_4^{2-} + 6H_2O$				
(Estimated volumes, log K_{so}^{o}, $\Delta_f G^{\circ}$ values)		*380*	*−97.6*	*−11,192.2*	ts, [50]
$CaAlH(PO_4)_2$	$6H_2O \Leftrightarrow Ca^{2+} + H^{+} + Al^{3+} + 2PO_4^{3-} + 6H_2O$	163.6	−45.1	−4735.3	ts, [51]
Bearthite	$Ca_2Al(PO_4)_2OH + H^{+} \Leftrightarrow 2Ca^{2+} + Al^{3+} + 2PO_4^{3-} + H_2O$	95.26	−30.65	−4038.7	[52,53]
Millisite	$KCaAl_6(PO_4)_4(OH)_9{\cdot}3H_2O + 9H^{+} \Leftrightarrow K^{+} + Ca^{2+} + 6Al^{3+} + 4PO_4^{3-} + 12H_2O$				
(Estimated log K_{so}^{o} and $\Delta_f G^{\circ}$ values)		281.3[f]	*−58.8*[f]	*−10,994.0*	ts, [54]
Ca-Millisite	$Ca_{1.5}Al_6(PO_4)_4(OH)_9{\cdot}3H_2O + 9H^{+} \Leftrightarrow 1.5Ca^{2+} + 6Al^{3+} + 4PO_4^{3-} + 12H_2O$				
(Estimated log K_{so}^{o} and $\Delta_f G^{\circ}$ values)		281.3[f]	*−47.9*[g]	*−10,925.7*	ts
Crandallite	$CaAl_3(PO_4)_2(OH)_5{\cdot}H_2O + 5H^{+} \Leftrightarrow Ca^{2+} + 3Al^{3+} + 2PO_4^{3-} + 6H_2O$	138.2	−35.9[h]	−5669.2	ts, [55]
Montgomeryite	$Ca_2Al_2(PO_4)_3(OH){\cdot}7H_2O + H^{+} \Leftrightarrow 2Ca^{2+} + 2Al^{3+} + 3PO_4^{3-} + 8H_2O$				
(Estimated log K_{so}^{o} and $\Delta_f G^{\circ}$ values)		454.3	*−57.4*[i]	*−7354.0*	ts, [56]

[a] Mean value of $10^{-24.84}$ [35], $10^{-25.4\pm0.7}$ (recalculated from experimental values reported in [57]), and $10^{-25.1\pm2.1}$ (recalculated from experimental values reported in [58]). The stability of Al-PO_4 is strongly influenced whether the formation of Al-PO_4 complexes is considered or not; neglecting the formation of Al-PO_4 complexes increases the solubility of variscite by approximately 3 log units. Based on the $\Delta_f G^{\circ}$ (−2120.0 kJ/mol) derived here, and the heat capacity (166.0 J/mol/K) and entropy (134.5 J/mol/K), both determined by [59], an enthalpy $\Delta_f H^{\circ}$ of −2362 kJ/mol was calculated.

[b] Mean values from the recalculated solubility products based on the experimental data reported in Webber [60]: $10^{-23.1\pm0.2}$ and based on Taylor and Gurney: $10^{-24.2\pm1.5}$ [61], $10^{-23.8\pm1.8}$ [62]. Based on the $\Delta_f G^{\circ}$ (−2112.0 kJ/mol) derived here, and the heat capacity (166.0 J/mol/K) and entropy (134.5 J/mol/K), both determined by [59] for variscite, an enthalpy $\Delta_f H^{\circ}$ of −2354 kJ/mol was calculated for amorphous aluminum phosphate.

[c] Estimated from augelite and water, following the procedure outlined by De Lima and Reymao [63], a heat capacity of 226.3 J/mol/K and entropy 190.8 J/mol/K were estimated using structural water following the procedure outlined in [64].

[d] Recalculated formation constants based on the experimental data reported in Taylor and Gurney [65]. Based on the $\Delta_f G^{\circ}$ (−16,769.5 kJ/mol), and the heat capacity (1482.4 J/mol/K) and entropy (1404.2 J/mol/K), both determined by [66], an enthalpy $\Delta_f H^{\circ}$ of −18,896 kJ/mol was calculated, in good agreement with the measured $\Delta_f H^{\circ}$ of −18,924 ± 21 kJ/mol [66].

[e] Recalculated formation constants based on the experimental data reported in Taylor and Gurney [67]. Based on the $\Delta_f G^{\circ}$ (−4263.0 kJ/mol) derived here, and the heat capacity (320.2 J/mol/K) and entropy (294.7 J/mol/K), both determined by [68], an enthalpy $\Delta_f H^{\circ}$ of −4670 kJ/mol was calculated.

[f] log K = −58.82 estimated by Nriagu [69]; a heat capacity of 812.2 J/mol/K and entropy 721.7 J/mol/K was estimated from crandallite, minyulite and gibbsite following the procedure outlined in [64]. The provided density taken from [54] refers to a millisite $Na_{0.75}K_{0.25}CaAl_6(PO_4)_4(OH)_9{\bullet}3H_2O$ of natural origin also containing sodium. The density of Ca-millisite $Ca_{1.5}Al_6(PO_4)_4(OH)_9{\cdot}3H_2O$ was not available in literature. It was assumed to be same as that of millisite $Na_{0.75}K_{0.25}CaAl_6(PO_4)_4(OH)_9{\bullet}3H_2O$ in this study.

[g] log K = −47.91 estimated by Vieillard et al. [45]; a heat capacity of 801.3 J/mol/K and entropy of 694.0 J/mol/K was estimated from crandallite, berlinite, variscite and gibbsite following the procedure outlined in [64].

[h] log K = −28.36 estimated by Nriagu [69] for the reaction $CaAl_3(PO_4)_2(OH)_5{\cdot}H_2O + 5H^{+} \geq Ca^{2+} + 3Al^{3+} + 2PO_4^{3-} + 6H_2O$. A considerably more stable crandallite with log K = −35.86 was calculated from the solubility measurements between pH 6.9 to 9.8 given in [70]. A heat capacity of 404.5 J/mol/K and entropy of 356.9 J/mol/K was estimated from berlinite, variscite, portlandite, and gibbsite following the procedure outlined in [64].

[i] log K = −57.39 estimated by Nriagu [69]; a heat capacity of −613.7 J/mol/K and entropy of 580.5 J/mol/K was estimated from bearthite, variscite and structural water following the procedure outlined in [64].

[*] ts: calculated in this study. Estimated values are given in italics.

calorimeter reached thermal equilibrium. The internal wet-mixing was then carried out for 2 min. Duplicated samples were measured for each mix.

2.2.4. Electrical conductivity and pH measurement

Electrical conductivity and pH of the cement suspensions without or with aluminum sulfate ($Al_2(SO_4)_3{\cdot}16H_2O$) were monitored using the experimental setup described in [2]. The pH electrode (Mettler Toledo) was calibrated against pH buffers at 4, 7, 9 and 12 before use. The dry mixture of magnesium and KH_2PO_4 was well mixed before being added to the deionized water without or with aluminum sulfate ($Al_2(SO_4)_3{\cdot}16H_2O$) dissolved. As detailed in [2], the prepared cement suspension was stored in a vessel with a lid locked tightly to avoid possible carbonation and water evaporation during test. An overhead stirrer was used to mix continuously the cement suspension until the end of the test after 24 h. Also a water bath at 20 °C was used to ensure a thermal stable environment. Data of both electrical conductivity and pH of the investigated cement suspensions were recorded automatically at time steps of 1 min.

2.2.5. Solution composition

The investigated cement suspensions were prepared and mixed continuously using an overhead stirrer within the first 24 h, afterwards they were continuously mixed using a horizontal shaker, which led to some agglomeration after 131 and 150 days. The liquid phases of the suspensions after specific reaction times were obtained through filtration using nylon filters with a mesh size of 0.45 μm. One part of the filtered solution was diluted using Milli-Q water and measured by ion chromatography (IC, Dionex DP series ICS-3000) to determine the concentrations of sodium [Na], potassium [K], magnesium [Mg], calcium [Ca], aluminum [Al], sulfate [SO_4] and phosphate [PO_4] ions. The other part of the solution was used for pH measurement. The pH meter (Meter 766) was calibrated against pH buffers at 4 and 12 before use.

2.2.6. Analyses of solid samples

To trace the evolution of solid assemblages in the investigated hydrating pastes, hydration was stopped after specific reaction times [24]. The pastes were crushed gently into small pieces and soaked in isopropanol for around 15 min. Afterwards isopropanol was removed by filtration, and diethyl ether was used to rinse the solids and removed by filtration. The obtained solids were further dried at 40 °C for around 10 min to remove any remaining organic solvents, and were then stored in sealed bottles. The solid samples were ground by hand to powders with grain size below 63 μm before further analyses by X-ray diffraction (XRD), thermogravimetric analyses (TGA), and solid-state nuclear magnetic resonance (NMR) spectroscopy.

The XRD analyses were performed with a PANanlytical X'Pert Pro in a θ-θ configuration using CoKα radiation and the X'Celerator detector. All powder samples were scanned between 5 and 90° 2θ for 45 min. TGA analyses were performed using a Mettler Toledo TGA/SDTA 851e instrument under nitrogen atmosphere. The weights of all samples were measured over the temperature range from 30 to 600 °C at a heating rate of 10 °C/min in 150 μL alumina crucibles. Following the method detailed in [23,25,26] and based on the XRD and TGA results, the reaction degree of magnesia [α_{MgO}] in the hydrating pastes was calculated. The corresponding XRD and TGA data of the reference paste P4-R for the calculations are from [23], and those for the paste with aluminum sulfate P4-AlS are based on the results presented here.

The NMR spectra were recorded on a Bruker Avance III HD 400 MHz wide-bore spectrometer using a 2.5 mm CP MAS NMR probe. Single plus ^{27}Al (^{31}P) MAS-NMR data of 10–14 mg of dried material were acquired at rotation rates of 25 kHz at 104.3 (162.0) MHz with 1 (2.5) μs corresponding to 15 (90)° excitations, and the applied recycle times of 1 (10) s ensured quantitative acquisition of the spectra. Chemical shifts of ^{27}Al and ^{31}P were referenced to the external standards of 1.1 M solution of Al $(NO_3)_3$ in D_2O and to solid $NH_4H_2PO_4$ at 0.0 ppm, respectively.

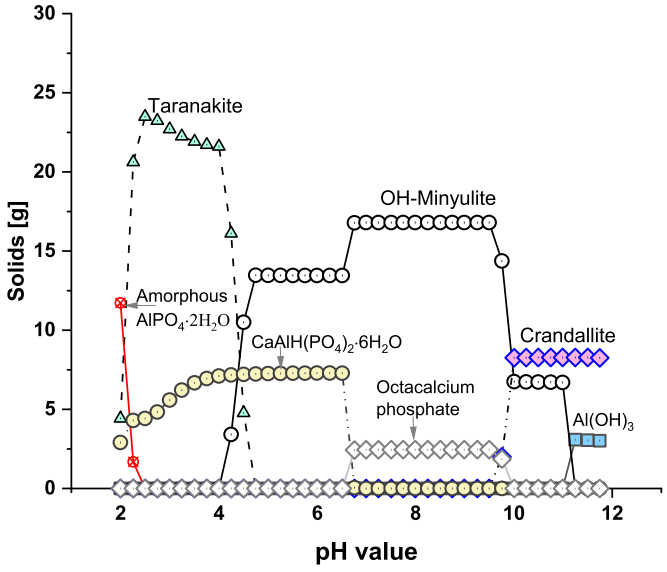

Fig. 1. Calculated effect of pH on the hydrates formed and speciation in a solution containing 200 mM H_3PO_4, 100 mM $Al(OH)_3$, 10 mM $Ca(OH)_2$ and increasing amounts of KOH.

Furthermore, deconvolution of the ^{27}Al MAS NMR spectra was carried out to obtain relative proportions of octahedrally and tetrahedrally coordinated Al by non-linear least-square fits using the "DMFIT" software developed by Massiot [27]. Generally, the fitting of the ^{27}Al NMR octahedral sites was performed using i) a Lorentzian shape at 9 ppm (line width of ca. 1.1 kHz) and ii) a quadrupolar broadened shape using the "Czjzek simple" [28] model starting with the parameters FWHM CS = 8 ppm (FWH CS = full width at half maximum of the isotropic chemical shift Gaussian distribution), CQ = 4–5 MHz CQ = (peak value of the quadrupolar coupling of the Czjzek/GIM distribution) and d = 5 (exponent of the Czjzek distribution). The resonances at the tetrahedral Al sites were fitted with the "Czjzek simple" model as well (parameters FWHM CS = 11 ppm, CQ ~ 4.5–5.5 MHz and d = 5). A very detailed step-by-step description of the procedure for fitting the line shape of ^{27}Al MAS NMR data of disordered phases can be found in the supporting information to one of our previous publications [29]; also typical examples of the simulated ^{27}Al MAS-NMR data are provided in Appendix A.

2.2.7. Thermodynamic modelling

Thermodynamic modelling was used to calculate the thermodynamically stable phases in the hydrating MKP cements without/with aluminum sulfate ($Al_2(SO_4)_3{\cdot}16H_2O$). The geochemical software GEMS-PSI [30] was used together with the Nagra/PSI geochemical database [31], the cement-specific Cemdata18 [32], and the magnesium (potassium) and calcium phosphate database (phosphate database) [19,23,33]. The database was extended with thermodynamic data for aluminum and phosphate containing aqueous complexes and solids as summarized in Table 3. Different aqueous Al-complexes might form based on the experimental investigations of Ciavatta and co-workers [34,35]: $Al(H_2PO_4)_2^+$, $AlH_2PO_4^{+2}$, $AlHPO_4^+$ and $AlPO_4^0$. At pH values above pH 4 the uncharged $AlPO_4^0$ complex is the dominant species (see Appendix B, Fig. B-1). Note that the uncharged $AlPO_4^0$ and $Al(H_2PO_4)_2^+$ species are missing in most of the commonly used databases [36–38] and that most solubility products reported in those databases were derived by neglecting the existence of Al-phosphates complexes. The positively charged polynuclear complexes ($Al_3H_3PO_4^{+3}$, $Al_3H(PO_4)_2^{+4}$, $Al_3H_3(PO_4)_3^{+3}$, $Al_3H(PO_4)_3^+$, $Al_3H_6(PO_4)_4^{+3}$, $Al_3H_7(PO_4)_5^+$) determined in Ciavatta [34] occur only at pH values below 4 (see Appendix B, Fig. B-2) and are thus not further considered. Negatively charged aluminum phosphate hydroxide complexes, which might form at higher

pH values, are not reported in literature.

Different Al-phosphates ($AlPO_4{\cdot}xH_2O$) can precipitate from supersaturated solutions under acidic to neutral conditions as illustrated in Fig. 1 and Appendix B (Fig. B-3). At ambient temperature amorphous $AlPO_4{\cdot}2H_2O$ has been observed to form, while the formation of the thermodynamically more stable variscite, metavariscite or berlinite is kinetically hindered [60,71,72]. At 100 °C and above either metavariscite ($AlPO_4{\cdot}2H_2O$) or variscite ($AlPO_4{\cdot}2H_2O$) precipitate, while at ≥150 °C berlinite ($AlPO_4$) crystallizes with time [72,73]. The available thermodynamic data [6,38,39,57] suggest that variscite is the stable phase at below ~130 °C, while at temperatures above berlinite is stabilized. At 25 °C, the solubility of variscite is roughly 2.5 log units lower than that of berlinite [6,39].

Iuliano and co-workers [35] derived for the formation of **variscite** a solubility product of $10^{-24.84}$ for the reaction $AlPO_4{\cdot}2H_2O \Leftrightarrow Al^{3+} + PO_4^{3-} + 2H_2O$ (considering the presence of aqueous Al-phosphate complexes as detailed in Table 3). This solubility product is 2 to 3 log units more negative than the solubility product of $10^{-22.06}$ [6,38,57] or $10^{-21.0}$ [74] derived neglecting the formation of Al-phosphate complexes. A re-calculation of the experimental data measured taking into account the formation of the different Al-phosphate complexes resulted in $10^{-25.4\pm0.7}$ for the data of Lindsay et al. [57] and in $10^{-25.1\pm2.5}$ for the data of Cole and Jackson [58]. A mean value of $10^{-25.1}$ was selected for the solubility product of variscite as indicated in Table 3.

The solubility of **amorphous $AlPO_4{\cdot}2H_2O$** has been determined by [60–62,75,76] and was found to be roughly 2 to 3 log units more soluble than variscite [6,75,76]. Solubility products between $10^{-19.7}$ and $10^{-20.2}$ were reported in [60–62,75,76], where in all cases the formation of aqueous Al-phosphate complexes has been neglected. Chen et al. [76] interpreted the data as sorption of phosphate on $Al(OH)_3$ and not in terms of amorphous $AlPO_4{\cdot}2H_2O$, however, the constant ion activity product of $10^{-19.9}$ reported in [76] over a large range of experimental conditions indicates rather the formation of amorphous $AlPO_4{\cdot}2H_2O$ as e.g. reported also by [77]. The solubility product of amorphous $AlPO_4{\cdot}2H_2O$ was recalculated here based on experimentally determined concentrations reported in [60–62] resulting in mean solubility product of $10^{-23.7}$ for amorphous $AlPO_4{\cdot}2H_2O$ as compiled in Table 3.

In Al-rich systems, in addition augelite ($Al_2PO_4(OH)_3$), senegalite ($Al_2PO_4(OH)_3{\cdot}H_2O$), wavelite ($Al_3(PO_4)_2(OH)_3 \cdot 5H_2O$) and trolleite ($Al_4(PO_4)_3(OH)_3$) could potentially form. As for berlinite, the formation of augelite, wavelite and trolleite is generally observed at above ambient temperature and pressure [52,73,78] and they are thus not expected to form in the systems studied here.

In the presence of potassium, the formation of **taranakite** ($K_3Al_5(HPO_4)_6(PO_4)_2{\cdot}18H_2O$) and at pH values of 4 and above, the formation of a **minyulite-like** basic potassium aluminate phosphate ($KAl_2(PO_4)_2OH{\cdot}2H_2O$) has been observed [6,65,67], see Fig. 1. The latter phase forms at low pH and ambient temperature and has an orthorhombic structure [49]. It has the same chemical composition but a different crystal structure than tinsleyite, which forms at higher temperatures and neutral pH and has a monoclinic structure [79]. Taylor and Gurney [65] derived for taranakite a solubility product of $10^{-178.7}$ for the reaction $K_3Al_5(HPO_4)_6(PO_4)_2{\cdot}18H_2O \Leftrightarrow 3\ K^+ + 6H^+ + 5Al^{3+} + 8PO_4^{3-} + 18H_2O$, while [68] derived, based on measurements of the heat capacity and enthalpy, a solubility product of $10^{-187.1}$. For the minyulite-like phase a solubility product of $10^{-41.0}$ for the reaction $KAl_2(PO_4)_2OH{\cdot}2H_2O + H^+ \Leftrightarrow K^+ + 2Al^{3+} + 2PO_4^{3-} + 3H_2O$ has been derived [67]. Recalculations based on the experimental data reported in Taylor and Gurney [65,67] and considering the formation of Al-phosphate complexes resulted in solubility products of $10^{-190.1\pm2.4}$ for taranakite and $10^{-46.3}$ for the minyulite-like phase as compiled in Table 3.

For hydrotalcite (OH-LDH) the data suggested in the Cemdata18 database were selected [32]. For phosphate containing hydrotalcite (PO_4-LDH) no thermodynamic data or solubility measurements are available. Gillman et al. [80] and Liu et al. [81] both observed a strong stabilization of PO_4-LDH compared to nitrate-LDH. Based on their observations, for PO_4-LDH the same solubility was assumed as measured for carbonate-LDH with Mg/Al = 2, 3 and 4 [50], which is also a strongly stabilized compared to nitrate-LDH [80,81].

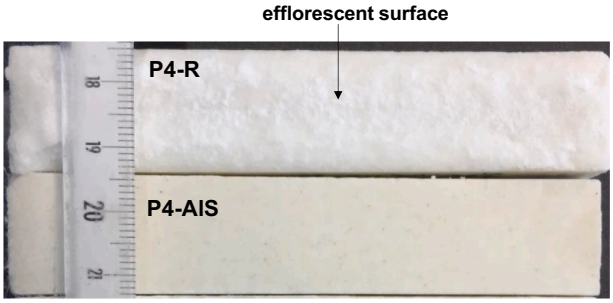

Fig. 2. Top surface conditions of the pastes P4-R and P4-AlS.

In the presence of Ca, **$CaAlH(PO_4)_2{\cdot}6H_2O$** might form under acidic conditions [62], see Fig. 1. Taylor and Gurney [62] measured their solubility and reported a solubility product of 10^{-39} for the reaction $CaAlH(PO_4)_2{\cdot}6H_2O \Leftrightarrow Ca^{2+} + H^+ + Al^{3+} + 2PO_4^{3-} + 6H_2O$. Recalculations based on the experimental data reported in Taylor and Gurney [62] considering the formation of Al-phosphate complexes resulted in a solubility product of $10^{-45.1\pm3.3}$. At very high temperatures bearthite could potentially form [52].

Under less acidic conditions the presence of millisite ($KCaAl_6(PO_4)_4(OH)_9{\cdot}3H_2O$, $Ca_{1.5}Al_6(PO_4)_4(OH)_9{\cdot}3H_2O$) is expected. At higher pH values rather crandallite ($CaAl_3(PO_4)_2(OH)_5{\cdot}H_2O$) or, at high phosphate concentrations (>~1 mM), montgomerite ($Ca_2Al_2(PO_4)_3(OH){\cdot}7H_2O$) are formed. At high pH values, Ca-phosphates such as hydroxyapatite, octacalcium phosphate or brushite, and $Al(OH)_3$ are expected to be stabilized [69,82] as also illustrated in Fig. 1. Thermodynamic data for millisite, crandallite and montgomerite have been estimated by [83], those for Ca-millisite by [45], those data are associated with a considerable uncertainty and are labelled as tentative in Table 3. A few experimentally solubility data are available only for crandallite [70].

In addition, the occurrence of foggite ($Ca_2Al_2(PO_4)_2(OH)_4{\cdot}3H_2O$) has been observed naturally in pegmatites [84]. No thermodynamic data for foggite are available in literature.

Fig. 1 illustrates the sequence of solid Al- and Ca-phosphates expected to form as a function of pH in a system containing 200 mM H_3PO_4, 100 mM $Al(OH)_3$, 10 mM $Ca(OH)_2$ and increasing amount of KOH. In the absence of KOH, variscite or amorphous $AlPO_4{\cdot}2H_2O$ (if variscite formation is suppressed due to kinetic reasons) are stable, while in the presence of 10 mM KOH and above, the formation of taranakite ($K_3Al_5(HPO_4)_6(PO_4)_2{\cdot}18H_2O$) and $CaAlH(PO_4)_2{\cdot}6H_2O$ is anticipated. At pH above 4 taranakite is expected to be destabilized to minyulite-like basic potassium aluminate phosphate ($KAl_2(PO_4)_2OH{\cdot}2H_2O$), at pH above 10 crandallite ($CaAl_3(PO_4)_2(OH)_5{\cdot}H_2O$) and at pH of 11 and above the formation of microcrystalline $Al(OH)_3$ (or gibbsite) can be expected. $CaAlH(PO_4)_2{\cdot}6H_2O$ is expected to be destabilized to hydroxyapatite or octacalcium phosphate (if apatite formation is suppressed due to kinetic reasons). In the absence of calcium, the sequence of Al-based phosphate remains the same, with exception that no $CaAlH(PO_4)_2{\cdot}6H_2O$, octacalcium phosphate and crandallite ($CaAl_3(PO_4)_2(OH)_5{\cdot}H_2O$) can be formed as detailed in Appendix B (Fig. B-3). The concentration and speciation of Al in solution is strongly influenced by the presence of phosphate, while Al has little effect on the phosphate speciation due to its much lower solubility (see Appendix B, Fig. B-1, 2). The speciation and the solids formed will be further influenced by the presence of magnesium. In magnesium dominated systems, newberyite ($MgHPO_4{\cdot}3H_2O$) is stabilized up to pH ~7, while in the intermediate range cattiite ($Mg_3(PO_4)_2{\cdot}22H_2O$) and K-struvite ($MgKPO_4{\cdot}6H_2O$) at pH values above 8 are stabilized as discussed in [33].

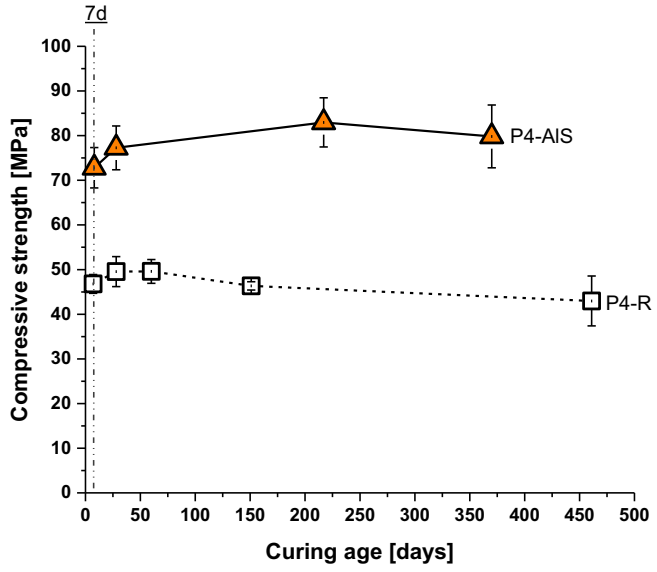

Fig. 3. Compressive strength evolution of the pastes P4-R and P4-AlS. Data of the reference paste P4-R are taken from [18].

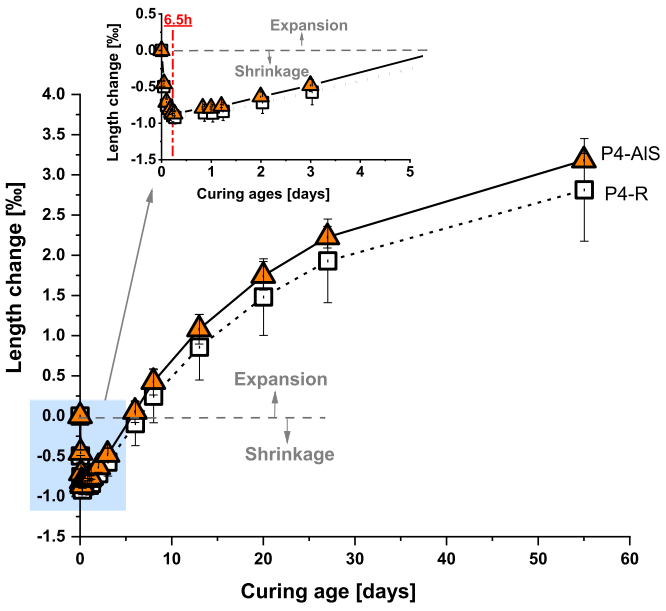

Fig. 4. Length change of the pastes P4-R and P4-AlS stored at 20 °C and R.H. 70%. Data of the reference paste P4-R are taken from [18].

3. Results and discussion

3.1. Efflorescence, compressive strength and volume stability

As displayed in Fig. 2, the reference MKP cement paste P4-R shows an efflorescent and rough surface. In contrast, the paste with aluminum sulfate P4-AlS shows a smooth and clear surface, indicating that aluminum sulfate affects the reactivity and/or the hydrates formed in MKP cements.

Fig. 3 displays the compressive strength developments of the pastes. The reference paste P4-R shows a high strength of 47 MPa already after 7 days and has small strength changes thereafter. The presence of aluminum sulfate in the paste P4-AlS leads to much higher strengths of >70 MPa at all the investigated ages, again suggesting a strong effect of aluminum sulfate on the cement hydration and microstructure.

Length changes of the pastes at 20 °C and R.H. 70% within the first two months are compared in Fig. 4. The pastes show quite similar trends of the length changes over time, with initial early shrinkage during the first 6.5 h and followed by gradual volume expansions over time. The sample expansions up to the investigated 55 days do not lead to strength reduction as demonstrated in Fig. 3.

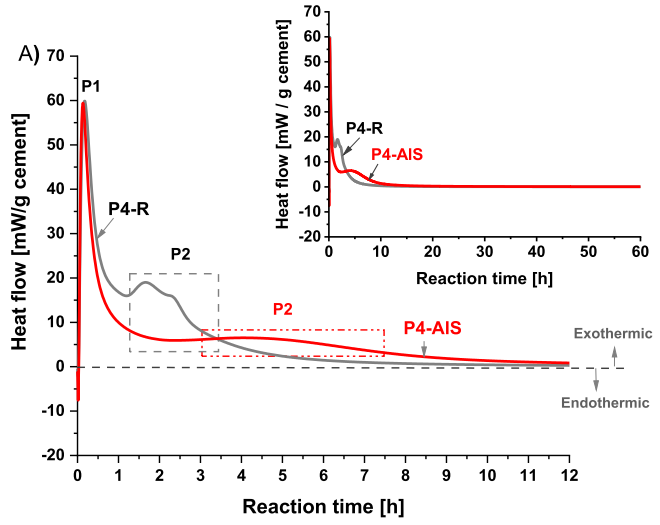

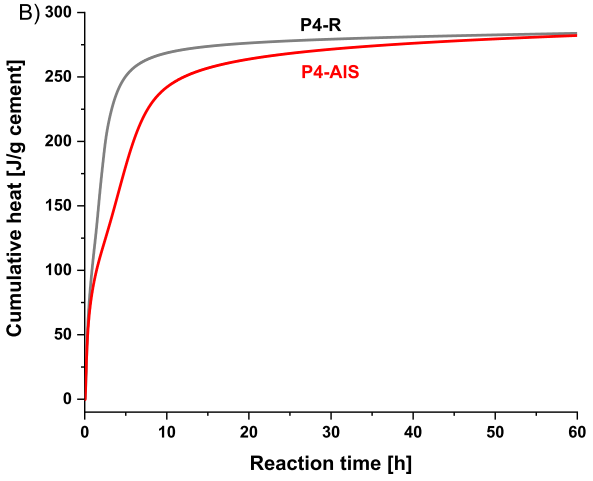

Fig. 5. A) Heat flow, and B) cumulative heat of the pastes P4-R and P4-AlS. Results of the heat flow and cumulative heat are normalized the weight of magnesia and KH_2PO_4, which is referred to as 'cement' in Y axis.

3.2. Reaction kinetics

3.2.1. Isothermal calorimetry of pastes

Isothermal calorimetry was used to study the effect of aluminum sulfate on the reaction progress in the pastes. The pastes without (P4-R) and with aluminum sulfate (P4-AlS) release most of their heat of hydration within the first day as shown in Fig. 5, suggesting very fast hydration reactions, consistent with the fast reactions observed for magnesia (see Fig. 10). Aluminum sulfate has no significant influence on the early hydration reaction during the first 1 h. However, aluminum sulfate strongly retards the 2nd exothermic hump (P2) from 2 h to around 4 to 6 h, showing the slowed down hydration reaction as also visible in the slower and gentler increase of the cumulative heat of the paste P4-AlS as displayed in Fig. 5B. However, the pastes reach similar total heat releases after around 60 h. These findings are in good agreement with the longer final setting time of the aluminum sulfate-containing paste P4-AlS than that of the reference paste P4-R as given in Table 2, highlighting the retardation effect of aluminum sulfate, in good agreement with the

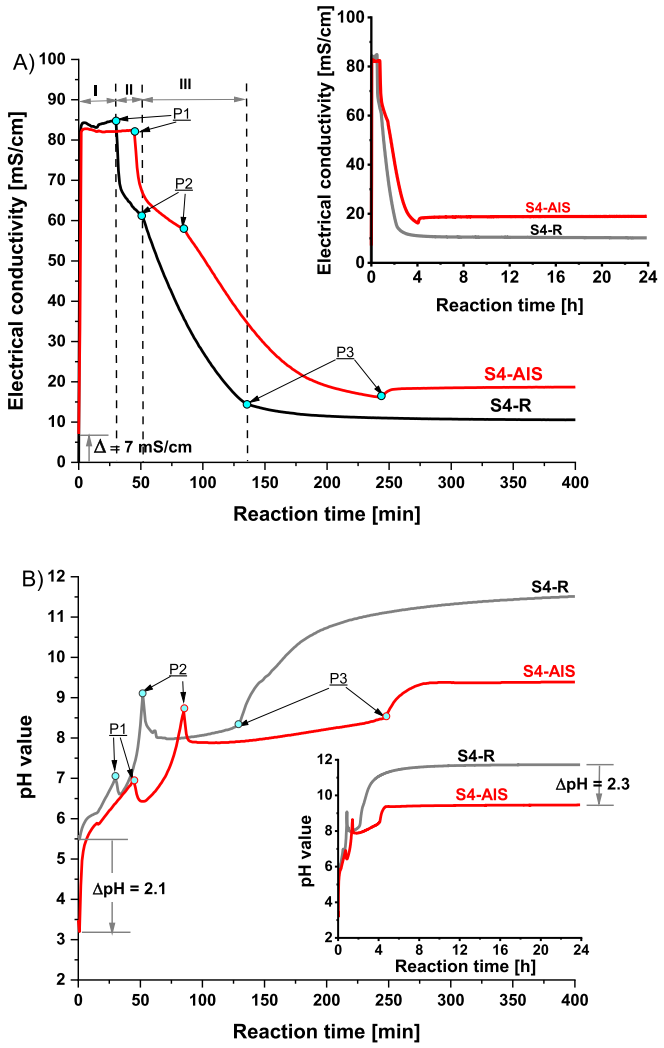

Fig. 6. A) Electrical conductivity, and B) pH development of MKP cement suspensions S4-R and S4-AlS.

findings at a lower Mg/PO_4 molar ratio of 1 in [6].

3.2.2. *Electrical conductivity and pH development of suspensions*

In addition to the pastes with a w/c ratio of 0.25, diluted suspensions with a w/c ratio of 5 were studied, which allowed to follow the changes in the aqueous phases continuously.

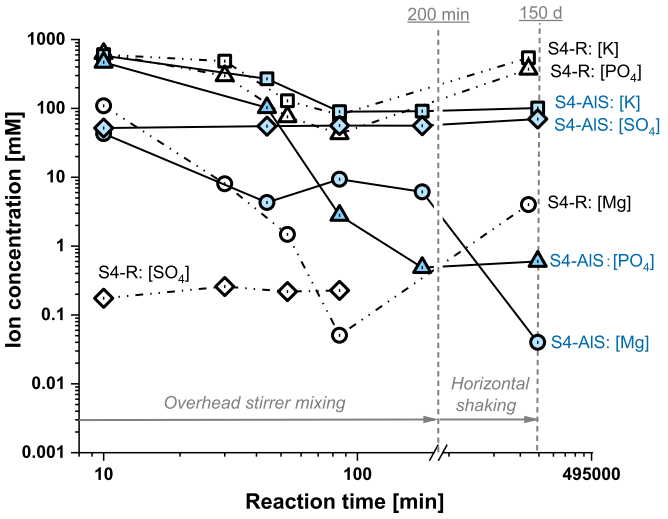

Fig. 7. Measured ion concentrations in the MKP cement suspensions S4-R and S4-AlS as a function of time.

As displayed in Fig. 6, the fast reactions between magnesia and KH_2PO_4 in the suspensions increase the electrical conductivity and pH values strongly as observed previously in [2,18]. The continuous precipitations of different hydrates and their transformations in the suspensions over time lead to the drops of electrical conductivity after the initial short constant stage (up to P1) and to the corresponding spikes of pH values. For the reference suspension S4-R, initially newberyite forms at low pH, followed by $Mg_2KH(PO_4)_2{\cdot}15H_2O$ and finally, along with an increase of the suspension pH, the sole hydrate of K-struvite was formed as evidenced by the XRD and TG results (see Appendix C) and as discussed in detail in [2,18].

The aluminum sulfate-containing suspension S4-AlS shows similar peaks and changes in the electrical conductivity and pH values, indicating a similar main hydration reaction as in the aluminum-free system S4-R. However, the presence of aluminum sulfate shifts the characteristic points (the labelled P1, P2 and P3) to later reaction times, indicating a slowdown in reaction, in good agreement with the isothermal calorimetry results of the pastes displayed in Fig. 5. A similar retardation effect was also reported for an aluminum nitrate-containing suspension with a lower Mg/PO_4 molar ratio of 1 and a higher w/c ratio of 100 [6].

Table 4
Elemental concentrations and pH values of the MKP cement suspensions S4-R and S4-AlS.

Time	[Na] mM	[K][a] mM	[Mg] mM	[Ca] mM	[Al][b] mM	[SO_4][b] mM	[PO_4][a] mM	pH[c]
S4-R								
10 min	4	605	109	3.6	<0.002	0.2	626	6.1
P1: 30 min	4	486	8	0.6	<0.002	0.3	298	7.6
P2: 53 min	4	129	1	0.1	<0.002	0.2	75	8.4
85 min	4	81	0.1	0.1	<0.002	0.2	43	10.6
131 d	n.a.	544	4	0.4	<0.002	n.a.	371	7.7
S4-AlS								
10 min	4	583	43	3.6	<0.002	52	467	6.1
P1: 45 min	4	269	4	0.1	<0.002	55	102	7.8
P2: 85 min	4	90	9	0.1	<0.002	56	3	8.4
3 h	4	91	6	0.1	<0.002	56	0.5	9.0
150 d	n.a.	101	0.04	0.02	<0.002	70	0.6	11.7

n.a.: not analyzed.

[a] The initial [K] and [PO_4] concentrations in S4-R and S4-AlS before reactions are 675 mM.

[b] The theoretical initial concentrations of [Al] and [SO_4] in S4-AlS before reaction should be 35 and 53 mM, respectively. The measured [SO_4] concentrations higher than 53 mM could be due to the sulfate impurities contained in the raw magnesia and/or KH_2PO_4 and to measurement error.

[c] The slight pH variations compared to those shown in Fig. 6B are within the error range, expect the values after 85 min for S4-R and after 3 h for S4-AlS are higher, which may be due to not-well controlled temperatures in the single experiments, leading to a faster reaction kinetics.

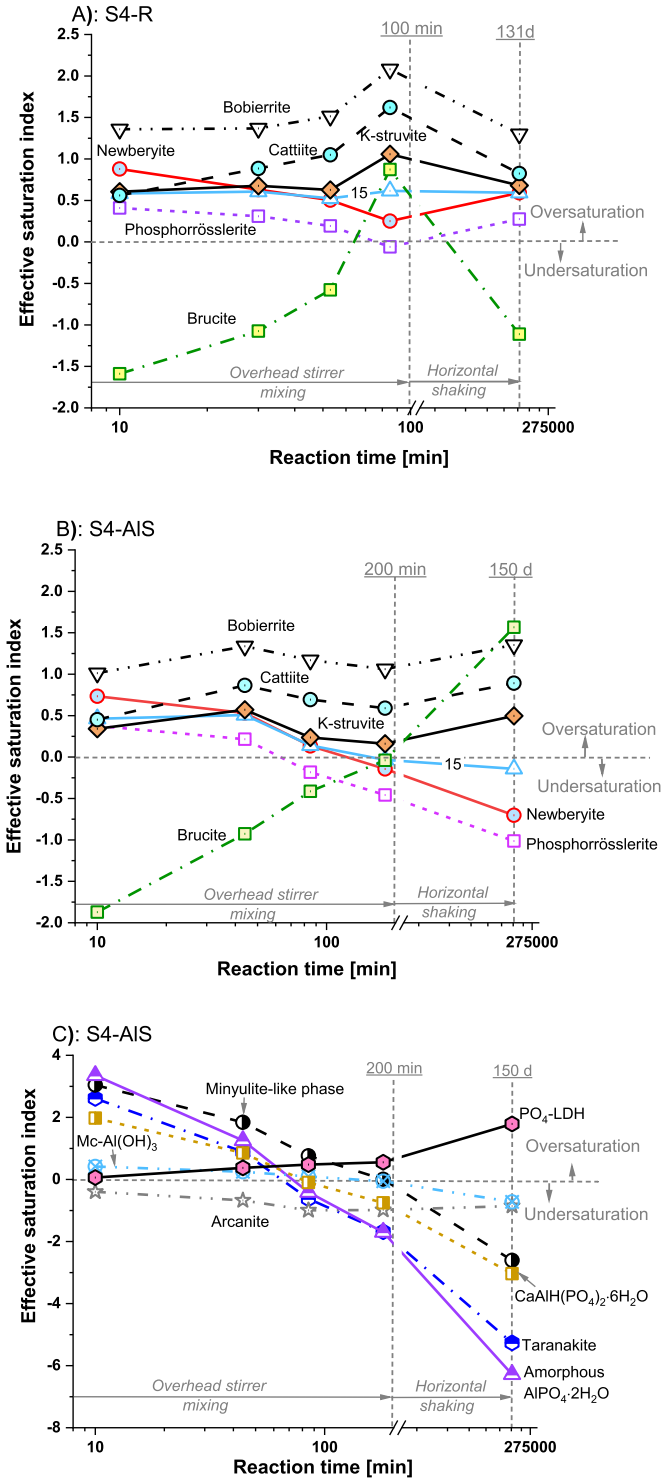

Fig. 8. Calculated effective saturation indices with respect to possible hydrate precipitations in: A) the reference suspension S4-R; B) and C) the aluminum sulfate-containing suspension S4-AlS. 15 = $Mg_2KH(PO_4)_2{\cdot}15H_2O$, Mc-Al$(OH)_3$ = microcrystalline $Al(OH)_3$.

Further the intrinsic acidic nature of aluminum sulfate reduces the initial solution pH by around two units as well as the pH values at later ages. Such a lower pH affects the hydrate formed as demonstrated in the following sections.

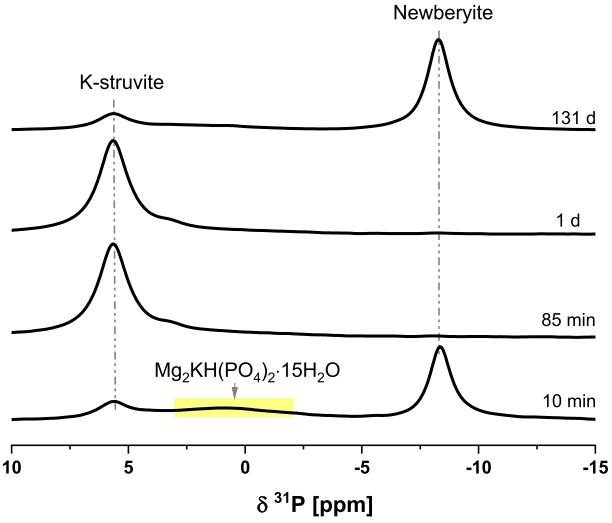

Fig. 9. ^{31}P MAS-NMR spectra of the reference MKP cement suspension S4-R with resonance assignments (compilation of ^{31}P and ^{27}Al NMR literature data in Table E, Appendix E). The yellow highlighted broad hump from around 3 to −2 ppm is assigned to $Mg_2KH(PO_4)_2{\cdot}15H_2O$. (For interpretation of the references to colour in this figure legend, the reader is referred to the web version of this article.)

3.3. Hydration of suspensions

3.3.1. Hydrate assemblages of the reference suspension

The measured ion concentrations in the suspensions over time are given in Table 4 and shown in Fig. 7. The [K], [Mg] and [PO_4] concentrations in the reference suspension S4-R decrease strongly within the first 85 min due to the initial precipitation of newberyite, followed by $Mg_2KH(PO_4)_2{\cdot}15H_2O$ and by K-struvite as demonstrated in Appendix C. According to the calculated effective saturation indices provided in Fig. 8A, brucite may precipitate in the suspension after 85 min and later as the suspension pH is above 10.6.

The analysis of the solid phases by XRD, TGA (see Appendix C) and ^{31}P MAS-NMR (see Fig. 9) show the formation of newberyite, K-struvite and $Mg_2KH(PO_4)_2{\cdot}15H_2O$ after 10 min. The on-going reaction of MgO leads within the first hour to the disappearance of newberyite and $Mg_2KH(PO_4)_2{\cdot}15H_2O$ and to formation of more K-struvite, indicating a phase transformation as also reported in [2,4,5,18]. No further changes were observed between 1 h and 1 day. An analysis of the suspension after 131 days, where agglomeration of the solids was observed, showed that K-struvite was partially destabilized to newberyite, while the pH decreased to 7.7. A similar destabilization of NH_4-struvite to newberyite after reaction times of 2 to 3 months has been reported previously [85]. In addition, to newberyite an additional unassigned water loss was observed by TGA (see Appendix C), while no other phases were identified by XRD or ^{31}P NMR.

3.3.2. Hydrate assemblages of the suspension with aluminum sulfate

For the suspension with aluminum sulfate S4-AlS, the initial aluminum concentration before reaction is around 34 mM (see Table 2); however, already after the first 10 min of reaction, it is decreased below the detection limit of 0.002 mM, suggesting the extremely fast precipitation of solid phases containing aluminum ions. Further the phosphate concentration of the suspension S4-AlS after the first 10 min are much lower compared to the reference suspension S4-R. The calculated effective saturation indices displayed in Fig. 8C indicate the possible precipitations of aluminum- and phosphate-containing phases during the first 10 min. The oversaturation follows the order amorphous $AlPO_4{\cdot}2H_2O$>minyulite-like phase ($KAl_2(PO_4)_2OH{\cdot}2H_2O$)>taranakite ($K_3Al_5(HPO_4)_6(PO_4)_2{\cdot}18H_2O$)>$CaAlH(PO_4)_2{\cdot}6H_2O$>microcrystalline Al

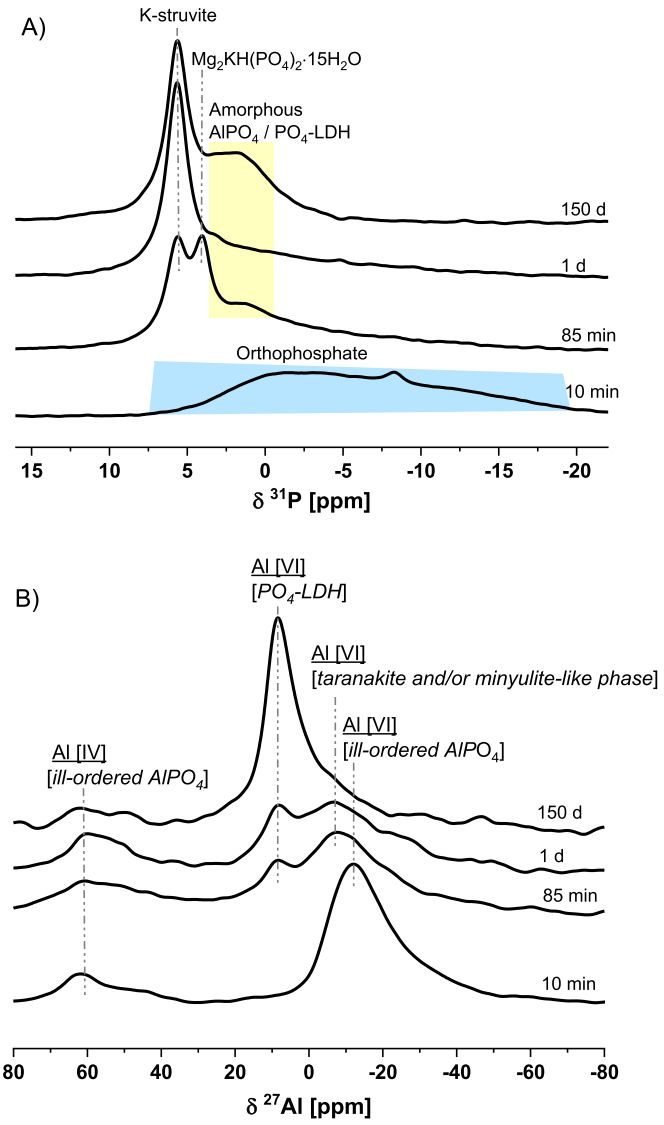

Fig. 10. A) ^{31}P and B) ^{27}Al MAS-NMR spectra of the MKP cement suspension prepared with aluminum sulfate S4-AlS with resonance assignments (compilation of ^{31}P and ^{27}Al NMR literature data in Table E, Appendix E).

$(OH)_3$. The lower magnesium concentration after the first 10 min could indicate a slowdown of MgO dissolution by aluminum sulfate, which would be consistent with the absence of any significant amount of magnesium phosphate hydrates observed by XRD, TGA and NMR as discussed in the next section. With time the pH values of the suspension increase while the calculated effective saturation indices in Fig. 8C decrease, such that amorphous $AlPO_4{\cdot}2H_2O$, taranakite, $CaAlH(PO_4)_2{\cdot}6H_2O$ and microcrystalline $Al(OH)_3$ are undersaturated after 50 min and the minyulite-like phase saturated after 3 h. In contrast, the saturation of PO_4-hydrotalcite increases, showing the potential for PO_4-LDH formation after 45 min and later. The concentration drops of potassium and phosphate concentrations with time are attributed to the formations of phosphorrösslerite, $Mg_2KH(PO_4)_2{\cdot}15H_2O$, cattiite and K-struvite and the transformations among them as demonstrated in the XRD and TG results given in Appendix D and as discussed in [2,4,5,18]. Compared to the reference suspension (S4-R), the solutions are less strongly oversaturated with respect to the different magnesium phosphates (see Fig. 8B). In addition, the concentration of sulfate ion remains almost constant throughout the whole investigated period indicating no significant uptake in solids, in good agreement with the calculated undersaturation of arcanite (K_2SO_4) given in Fig. 8C.

Table 5
^{27}Al isotropic chemical shifts and relative amounts of Al [VI] and Al [VI] sites and their tentative assignments obtained from the simulation of the MAS-NMR spectra of the S4-AlS and P4-AlS samples (suspensions and pastes of MKP cements in presence of aluminum sulfate).

Time	Al [IV]		Al[VI]a		Al [VI]b	
	Amorphous $Al(OH)_3$/ $AlPO_4$		PO_4-LDH		Tarakanite/minyulite-like phase	
	$\delta^{27}Al_{iso}$ [ppm]	rel. Int. [%]	$\delta^{27}Al_{iso}$ [ppm]	rel. Int. [%]	$\delta^{27}Al_{iso}$ [ppm]	rel. Int. [%]
S4-AlS						
10 min	69.0	16	–	–	−3.9[a]	84
85 min	69.0	27	8.2	20	0.2	53
1 d	65.8	23	7.9	28	0.4	49
150 d	66.4	11	7.9	68	3.0	21
P4-AlS						
1 h	58.0	12	5.5	19	−3.8[a]	70
1 d	58.0	16	5.7	20	−3.0[a]	64
28 d	57.7	31	6.0	6	−1.4	64
330 d	59.0	24	9.1	11	−1.0	65

[a] Tentatively assigned to amorphous $Al(OH)_3$ or aluminum phosphate. Note that for the broad Al [VI]b signal with a peak maximum at −12 ppm in the spectrum of 10 min (Fig. 10B) results due to second order quadrupolar interaction in an isotropic ^{27}Al NMR chemical shift of −3.9 ppm.

The analysis of the solid phases indicated the absence of significant amounts of crystalline hydrates after 10 min, and the formation phosphorrösslerite ($MgHPO_4{\cdot}7H_2O$) instead of newberyite ($MgHPO_4{\cdot}3H_2O$) (as observed in the absence of aluminum sulfate) after 20 min, followed by $Mg_2KH(PO_4)_2{\cdot}15H_2O$ during the first hour as demonstrated in the XRD and TG results given in Appendix D. Between 3 and 24 h cattiite ($Mg_3(PO_4)_2{\cdot}22H_2O$) and K-struvite formed, while after 150 days only K-struvite was observed, in agreement with high pH value of 11.7 observed (see Table 4), in contrast to the suspension without aluminum (S4-R). The same phases and trends were observed in ^{31}P MAS-NMR spectra (see Fig. 10A). The initial sample (10 min hydration time) showed a broad resonance between 7 and −20 ppm (the light blue highlighted area) indicating the presence of poorly ordered orthophosphates. After 85 min K-struvite is observed, together with an additional signal at 4 ppm, possibly related to $Mg_2KH(PO_4)_2{\cdot}15H_2O$, which is absent after 1 day and longer. At 1 and 150 days, mainly K-struvite is observed and in addition a broad shoulder from ~4 to ~0 ppm (the yellow highlighted area), which could be related to the presence of PO_4-LDH and/or amorphous aluminum phosphate as given in Table E (Appendix E). The characteristic resonance at 7 ppm reported for cattiite [5,6], expected after 1 day, is not clearly visible and might be overlapped by the dominating signal of K-struvite.

The ^{27}Al NMR spectrum (see Fig. 10B), which allows to specifically investigate the Al-containing phases, shows after 10 min a broad main resonance of octahedral Al [VI] with a maximum intensity at −12 ppm and a minor tetrahedral Al [IV] signal at ~60 ppm, which are possibly related to the formation of ill-ordered aluminum phosphate [6,86]. The Al [IV] is probably caused by to the rapid precipitation of a disordered structure (such as amorphous $Al(OH)_3$ or $AlPO_4$) containing both octahedral and tetrahedral aluminum as previously suggested by [6] and experimentally observed for rapid precipitating amorphous $AlPO_4$ [87]. The intensity of octahedral Al [VI] signal at −12 ppm decreases with time, and is replaced by a signal at −8 and a narrow and symmetric resonance at 8 ppm. The signal at −8 ppm could be related to the formation of taranakite and/or minyulite and was also observed in a recent study [6] on the effect of aluminum nitrate on MKP paste (Mg/PO_4 molar ratio = 1). A narrow and symmetric resonance at 8 ppm is commonly observed in samples containing LDH [50,81,88], while the signal of $Al(OH)_3$ although it occurs at a similar position, is generally broader and less symmetric [86,89–91]. In the sample aged for 150 days, ca. 70% of the Al is observed to be present at the resonance at 8 ppm (see

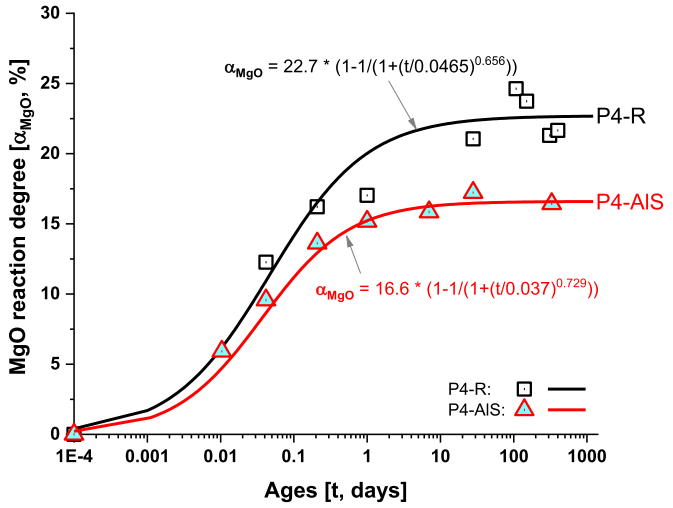

Fig. 11. Magnesia reaction degree [α_{MgO}]. The empty and filled symbols are the experimental values, and the solid lines present the derived relations to describe the magnesia reaction degree [α_{MgO}] as a function of age [t, days].

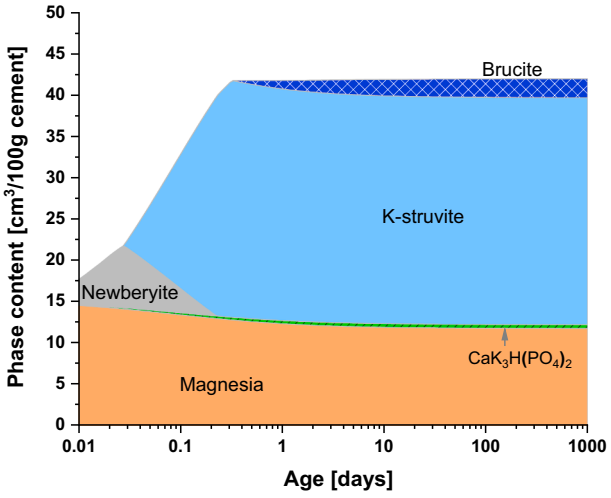

Fig. 12. Predicted phase evolutions of the reference paste P4-R. Note KH_2PO_4 initially present is mainly in solution and has partially reacted to newberyite.

Table 5), probably related to LDH formation, while 20% of Al is associated with the Al [VI] signal at −8 ppm, which possibly related to the formation of taranakite and/or minyulite [6,81]. In contrast to our observations, a recent study [6] on the effect of aluminum nitrate on MKP paste (Mg/PO_4 molar ratio = 1) showed only the presence of signal at −8 ppm (taranakite and/or minyulite-like phase), but no LDH signal, which could be related to the lower pH (<7.6) of that study. The presence of Al-sulfate in the suspension led not only to the formation of Al-containing phases (probably PO_4-LDH and taranakite and/or minyulite), but also promoted the formation of cattiite and phosphorrösslerite (instead of newberyite) as intermediate phase and stabilized K-struvite in the long-term.

3.4. Hydration of pastes

3.4.1. Dissolution kinetics of magnesia

The magnesia reaction proceeded relatively fast in the paste samples, as shown in Fig. 11. During the first day magnesia in both pastes reacts fast, which is consistent with the isothermal calorimetry results in Fig. 5. However, the reaction kinetics are slowed down thereafter.

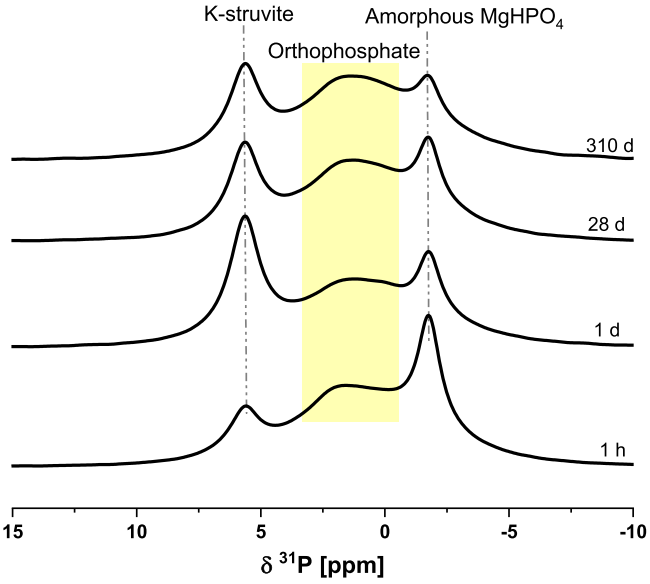

Fig. 13. ^{31}P MAS-NMR spectra of the reference MKP cement paste P4-R with resonance assignments (reported shifts for phosphates are compiled in Table E, Appendix E). The yellow highlighted broad hump from 3 to 0 ppm is assigned to bobierrite and/or amorphous $Mg_3(PO_4)_2$, possibly other orthophosphates. (For interpretation of the references to colour in this figure legend, the reader is referred to the web version of this article.)

Approximately 21% of the MgO have reacted in P4-R after 28 days and longer, only 17% of MgO had reacted in the P4-AlS, although the P4-AlS paste demonstrates significantly higher compressive strengths (see Fig. 3). This may indicate a potential important role of aluminum sulfate in formation of additional hydrates in the paste. As suggested by the TG results displayed in Appendix F (see Fig. F-2) and Fig. 16 A, both the pastes (P4-R and P4-AlS) show a similar amount of bound water after 28 days and longer.

3.4.2. Hydrate assemblages of the reference paste

Thermodynamically stable phases in the hydrating pastes over time were predicted using the thermodynamic data described in Section 2.2.7 and based on the derived magnesia dissolution kinetics as shown in Fig. 11. The modelling results in Fig. 12 indicate in the reference paste P4-R the initial precipitation of newberyite, its gradual destabilization to K-struvite, and the minor formation of brucite. Besides, traces of $CaK_3H(PO_4)_2$ are predicted in the paste as well, consistent with previous experimental observations in [18].

The phase compositions of the reference paste P4-R over time have been detailed in [23] based on XRD and TGA analysis and show that most KH_2PO_4 reacts with magnesia within the first day, leading to the formations of K-struvite and traces of bobierrite and brucite (see Appendix F). The phases are observed by ^{31}P MAS-NMR (see Fig. 13): the formation of increasing amount of K-struvite during the first day and of some bobierrite and/or amorphous $Mg_2(PO_4)_3$. An additional narrow resonance at −1.7 ppm is observed, which is assigned to amorphous $MgHPO_4$ [92]. The formation of amorphous $MgHPO_4$ has also been observed in pastes at ambient temperatures before [93], while in other sample struvite and newberyite had formed, indicating a similar stability of those phases. The experimental observations are in agreement with thermodynamic predictions (see Fig. 12) with the exception of the presence of some bobierrite, which seems to have formed as an intermediate phase, and the presence of amorphous $Mg_2(PO_4)_3$, which might be formed due to the lack of water available in the paste.

3.4.3. Hydrate assemblages of the paste with aluminum sulfate

With aluminum sulfate, the thermodynamic modelling of the paste

P4-AlS in Fig. 14 suggests a similar hydration process as for to the reference paste P4-R (see Fig. 12); moreover, additional hydrates such as taranakite ($K_3Al_5(HPO_4)_6(PO_4)_2{\cdot}18H_2O$) during the first hour, minyulite-like phase ($KAl_2(PO_4)_2OH{\cdot}2H_2O$) and arcanite ($K_2SO_4$) are also predicted to form. Taranakite and minyulite have also predicted been predicted for a MKP cement with Mg/PO_4 molar ratio = 1 [6]. Taranakite forms at low pH (see Fig. 1 and Appendix B) through the following equation

$$3\,K^+ + 5Al^{3+} + 8H_2PO_4^- + 18H_2O \rightarrow K_3Al_5(HPO_4)_6(PO_4)_2{\cdot}18H_2O + 10H^+ \quad (2)$$

But it is not stable above pH 4, where it is destabilized to minyulite-like phase:

$$2K_3Al_5(HPO_4)_6(PO_4)_2{\cdot}18H_2O + 17OH^- \rightarrow 5KAl_2(PO_4)_2OH{\cdot}2H_2O + K^+ + 6PO_4^{3-} + 38H_2O \quad (3)$$

Arcanite (K_2SO_4) is undersaturated in the suspension (S4-AlS) as suggested from the calculated effective saturation index in Fig. 8C, while in the paste with the much lower w/c ratio it is predicted to form, while in the paste in contrast to the suspensions, no PO_4-LDH phase is predicted to form.

Aluminum sulfate slows down early reaction in the paste (see Fig. 5), where mainly arcanite (K_2SO_4) is observed together with some K-struvite after the first 15 min (see Figs. 15A, 16A), while in the reference paste (P4-R) already a considerable amount of K-struvite and amorphous $MgHPO_4$ is present after 15 min (see Fig. 13, Appendices F and G). Arcanite remains in the matrix up to the investigated 330 days, in good agreement with the thermodynamic calculations in Fig. 14. After 300 days, in addition to K-struvite additional reflections at 22.1, 27.4 and 34.3° 2θ CoKα (d-spacing values = 4.6, 3.7 and 3.0 Å, respectively) appear as displayed in Fig. 15 as well as an additional weight loss in TGA (see Fig. 16A). The thermodynamic calculations in Fig. 14 predict the existence of a minyulite-like phase, however, this phase cannot be assigned unambiguously. More experimental evidences are needed for a further confirmation.

The TG results and ^{31}P MAS-NMR in Fig. 16 confirm the XRD findings and further reflect the presence of some unreacted KH_2PO_4 in the paste up to 5 h. The faster depletion of KH_2PO_4 compared to the that in the reference paste P4-R (see Appendix F) not only agrees well with observed fast precipitation of arcanite (K_2SO_4), but also explains the absence of efflorescence (see Fig. 2), as efflorescence normally occurs in MKP cements with a high availability of unreacted KH_2PO_4, like those with Mg/PO_4 molar ratios ≤5 [17,26]. The broad ^{31}P MAS-NMR signal observed between 1 and 300 days is assigned to the presence of amorphous $Mg_3(PO_4)_2$, possibly together with other phases such as phosphate adsorbed on $Al(OH)_3$ (~10 to −10 ppm) [81,94], PO_4-LDH (~10 to −10 ppm) [81], amorphous aluminum phosphate (~5 to −20 ppm) [94], and minyulite-like phase (~−7 to −19 ppm) [95,96].

As discussed above for the suspension, the ^{27}Al resonances with peak maxima at ~47, 8, and −9 ppm for pastes P4-AlS (see Fig. 17) indicate the initial formation of taranakite and/or minyulite-like phase (−9 ppm), while later ill-ordered aluminum phosphate (47, −12 ppm) as

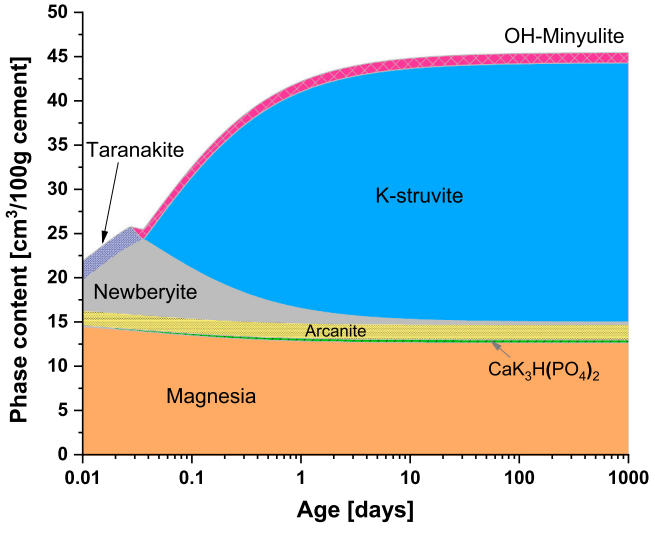

Fig. 14. Predicted phase evolutions of the paste prepared with aluminum sulfate P4-AlS.

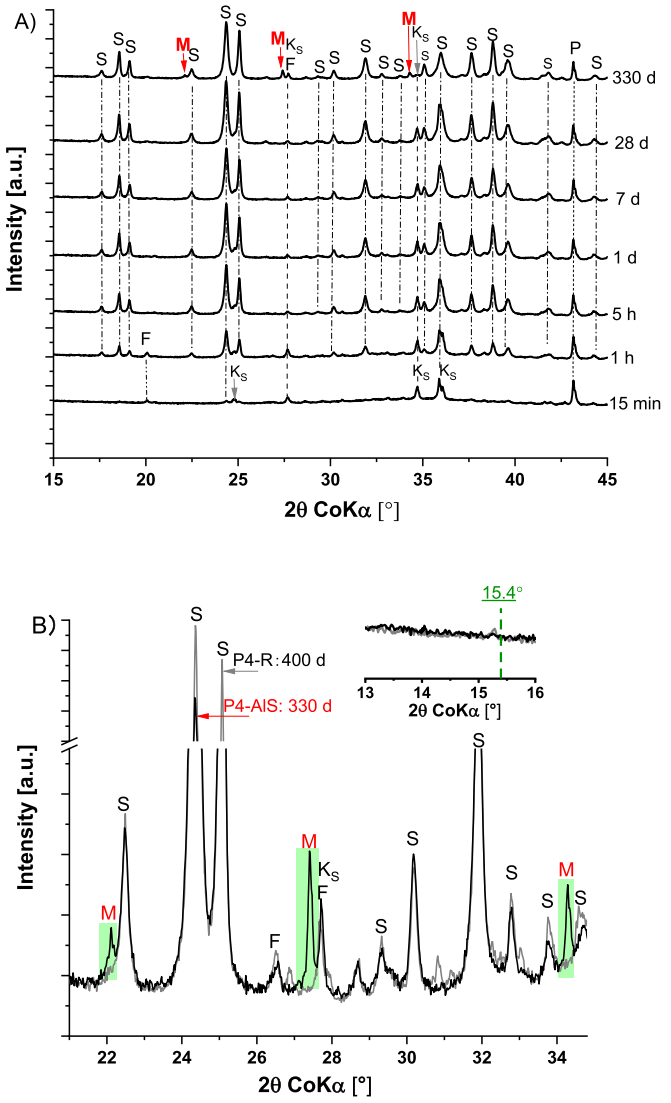

Fig. 15. A) XRD patterns of the paste prepared with aluminum sulfate P4-AlS. F = forsterite (Mg_2SiO_4), Ks = arcanite (K_2SO_4), M = reflections assigned to minyulite-like phase, P = periclase (MgO), S = K-struvite ($MgKPO_4{\cdot}6H_2O$). B) Detail of the XRD patterns of samples P4-R: 400 d (black) and P4-AlS: 330 d (grey) highlighting the reflections, which are tentatively assigned to the minyulite-like phase.

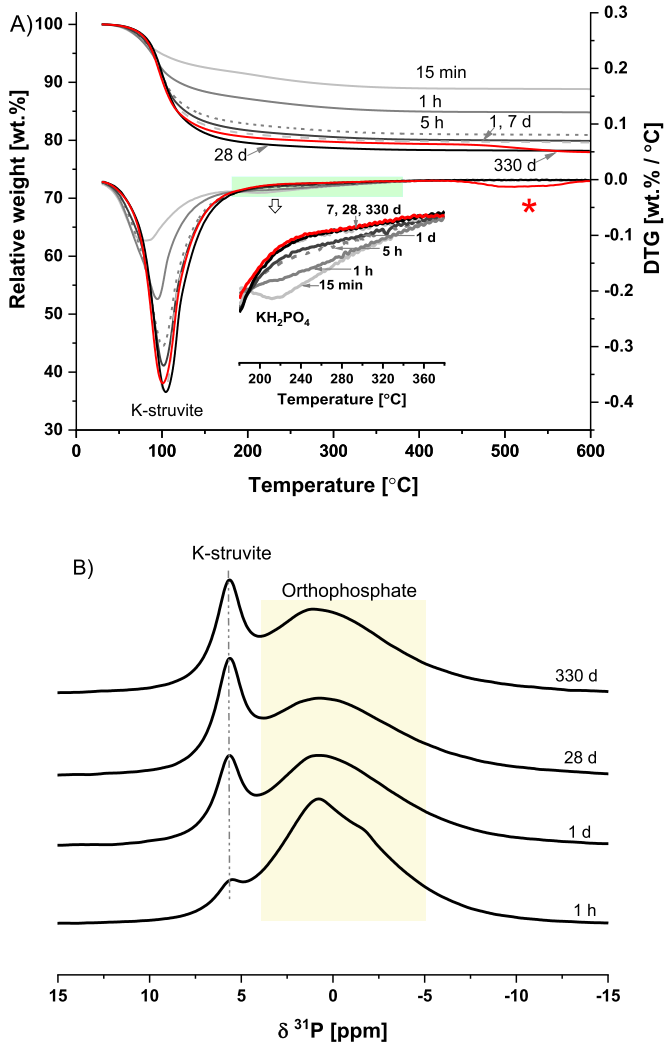

Fig. 16. A) TG/DTG curves (* = unassigned weight loss), and B) ^{31}P MAS-NMR spectra of the paste prepared with aluminum sulfate P4-AlS with resonance assignments (reported shifts for phosphates are compiled in Table E, Appendix E). The yellow highlighted broad hump from 4 to −5 ppm is assigned to unreacted KH_2PO_4 (after 1 h) and to amorphous $Mg_3(PO_4)_2$, possibly together with other orthophosphates. (For interpretation of the references to colour in this figure legend, the reader is referred to the web version of this article.)

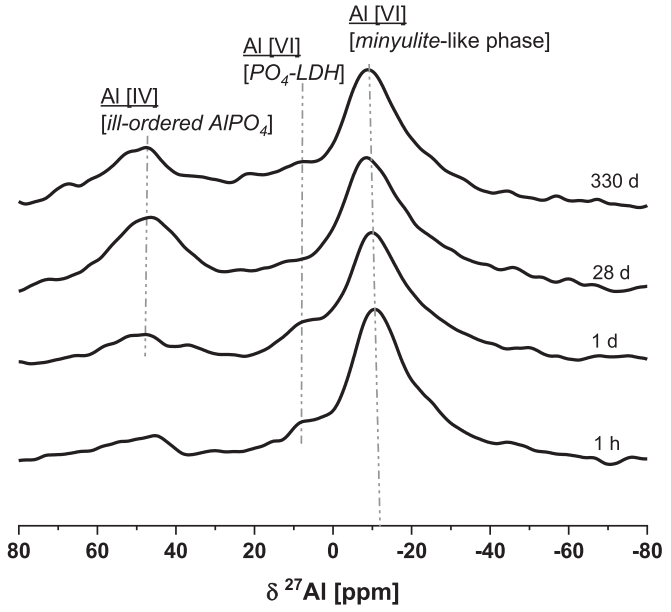

Fig. 17. ^{27}Al NMR spectra of the paste prepared with aluminum sulfate P4-AlS which chemical species assignments to PO_4-LDH, minyulite-like phase and to ill-ordered aluminum phosphate.

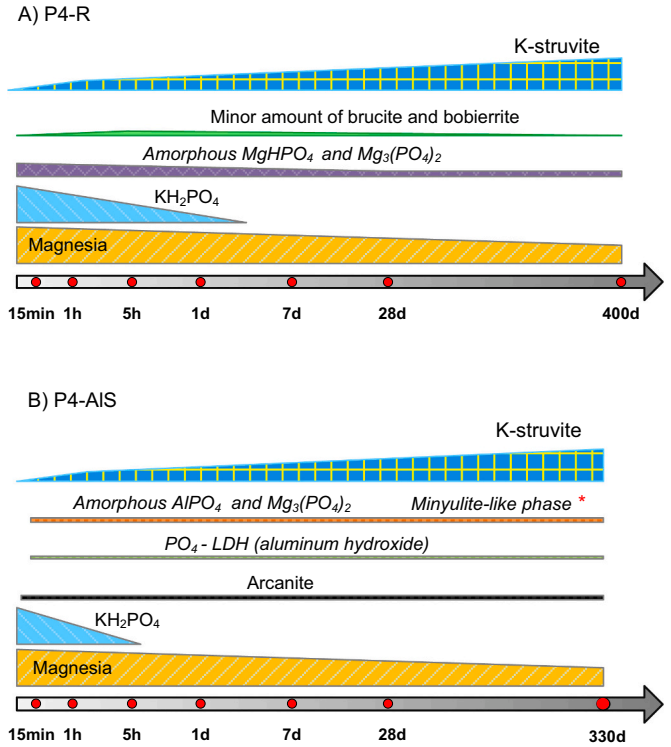

Fig. 18. Schematic drawing of the phase evolutions of the pastes without (P4-R) and with aluminum sulfate (P4-AlS). *: tentative assignment based on ^{27}Al MAS-NMR and thermodynamic modelling.

well as a small amount of PO_4-LDH (8 ppm) seem to be present. Little changes of the relative proportions of Al are observed (see Table 5) suggesting little changes after the first hour.

4. Conclusions

In this study, the influence of aluminum sulfate on properties and hydration of the MKP cement paste at an Mg/PO_4 molar ratio of 4 and a w/c ratio of 0.25 was investigated through a series of experimental characterizations and thermodynamic modelling. When compared with a reference paste, the presence of aluminum sulfate can slow down cement hydration kinetics, leads to a lower reaction degree of magnesia in the long-term, and thus to less magnesium-containing hydrates. In both pastes K-struvite and probably amorphous $Mg_3(PO_4)_2$ are the main hydrates (see Fig. 18). The presence of aluminum prevents the formation of amorphous $MgHPO_4$, bobierrite and brucite. Moreover, aluminum sulfate can lead to a faster and more complete depletion of KH_2PO_4 due to the formations of arcanite (K_2SO_4), amorphous aluminum phosphate, PO_4-LDH and possibly a minyulite-like phase. The increased consumptions of potassium and phosphate ions in the presence of aluminum sulfate could inhibit the efflorescence in the paste. Moreover, aluminum sulfate can increase paste compressive strength in both short- and long-term, but has little influences on the short-term paste volume stability.

CRediT authorship contribution statement

Biwan Xu: Conceptualization, Methodology, Investigation, Formal

analysis, Writing - Original Draft, Visualization.

Frank Winnefeld: Formal analysis, Writing - review & editing.

Bin Ma: Investigation, Formal analysis, Writing - review & editing.

Daniel Rentsch Investigation, Formal analysis, Writing - review & editing.

Barbara Lothenbach: Funding acquisition, Conceptualization, Formal analysis, Writing - Original Draft, Writing - review & editing.

Declaration of competing interest

The authors declare that they have no known competing financial interests or personal relationships that could have appeared to influence the work reported in this paper.

Acknowledgements

Saint-Gobain Recherche, France, is gratefully acknowledged for the financial support of Biwan Xu. The thanks are extended to Céline Cau Dit Coumes (CEA, France), Raül Leiva Muñoz and Nelly Brielles (Saint-Gobain Recherche, France) and Tao Liu (Tongji university, China) for many helpful discussions and suggestions. The NMR hardware was partially granted by the Swiss National Science Foundation (SNSF, grant no. 206021_150638/1).

Appendix A

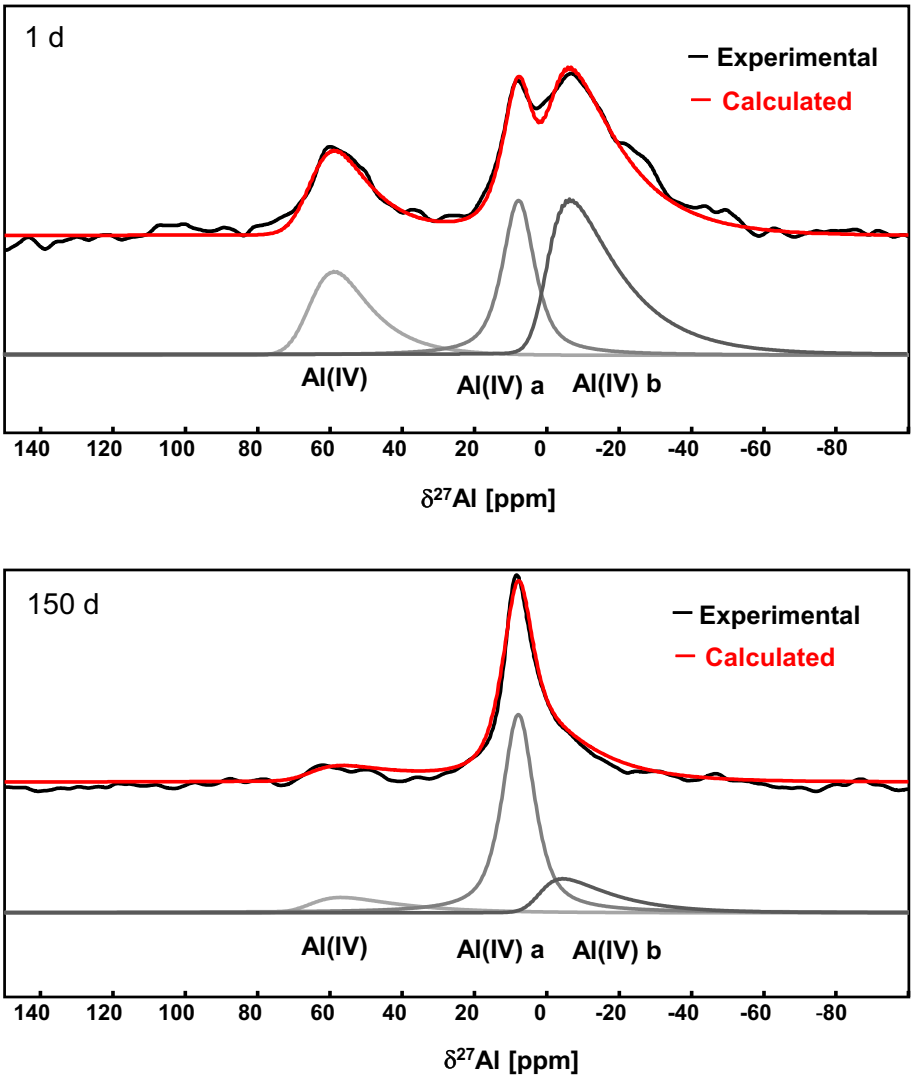

Fig. A. Typical examples of the experimental and simulated ^{27}Al MAS-NMR spectra of the MKP cement suspension S4-AlS after 1 and 150 days with simulated signals for the Al (IV), Al (VI)a and Al(VI)b sites.

Appendix B

Fig. B illustrates the sequence of solid Al-phosphates expected to form and the Al and phosphate speciation in solution in a system containing 100 mM H_3PO_4, 100 mM $Al(OH)_3$ and increasing amount of KOH to increase the pH values.

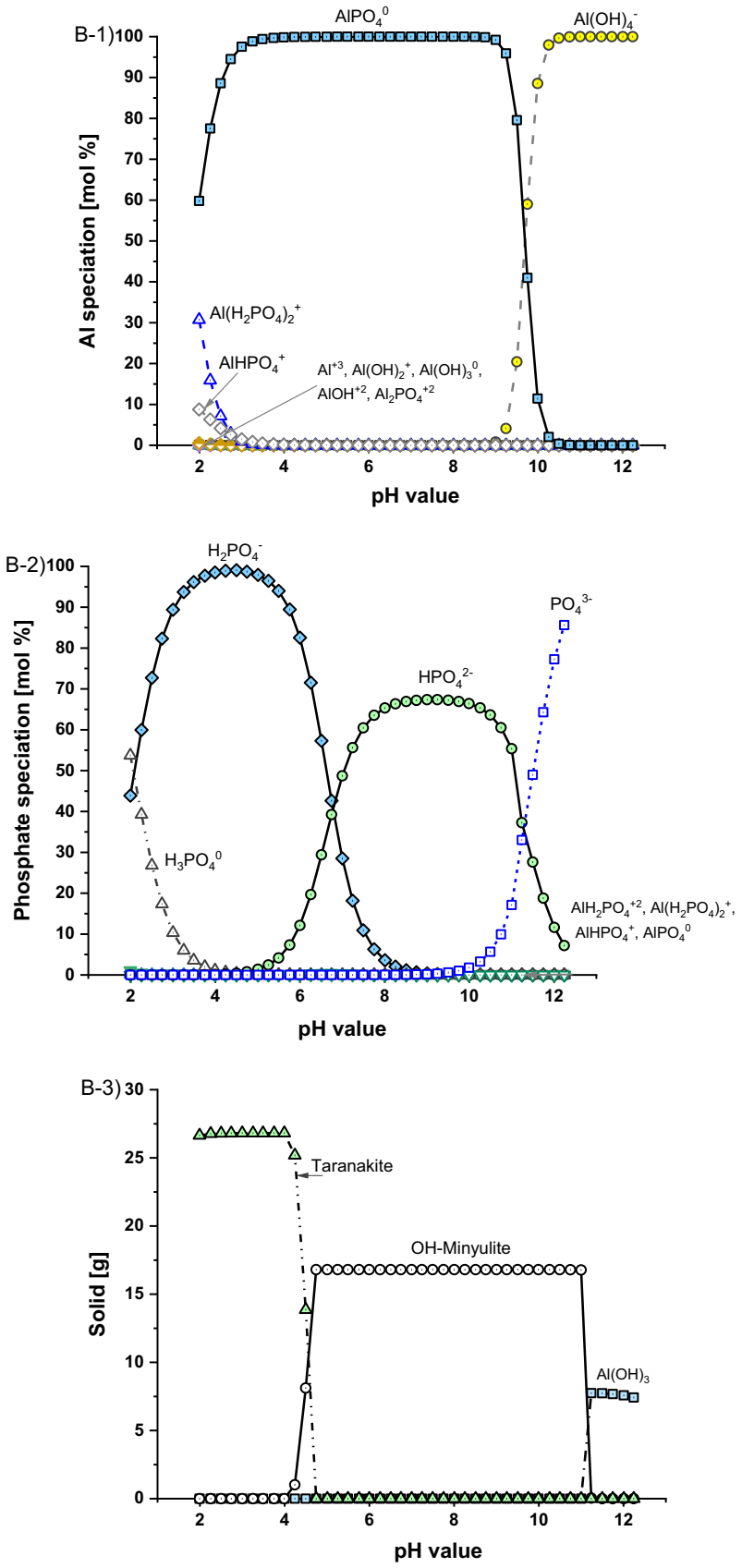

Fig. B. Calculated effect of pH on the hydrates formed and Al and phosphate speciation in a solution containing 200 mM H_3PO_4, 100 mM $Al(OH)_3$ and increasing amounts of KOH.

Appendix C

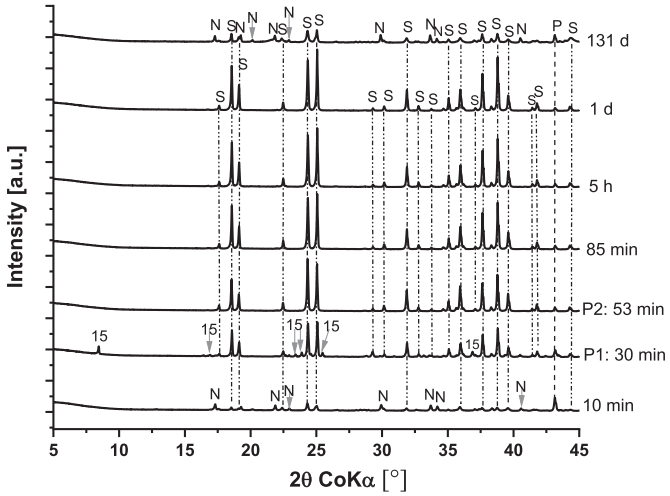

Fig. C-1. XRD patterns of the reference suspension S4-R over time. 15 = $Mg_2KH(PO_4)_2{\cdot}15H_2O$, N = newberyite ($MgHPO_4{\cdot}3H_2O$), P = periclase (MgO), S = K-struvite ($MgKPO_4{\cdot}6H_2O$). Note P1 and P2 are the two characteristic points as shown in Fig. 6.

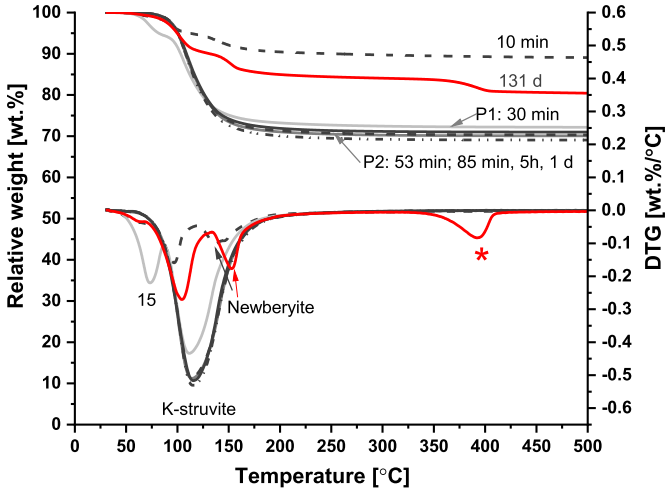

Fig. C-2. TG/DTG curves of the reference suspension S4-R over time. 15 = $Mg_2KH(PO_4)_2{\cdot}15H_2O$, * = unassigned weight loss (possibly remains of brucite, although not detected by XRD, and not expected at pH 7.7). Note P1 and P2 are the two characteristic points as shown in Fig. 6.

Appendix D

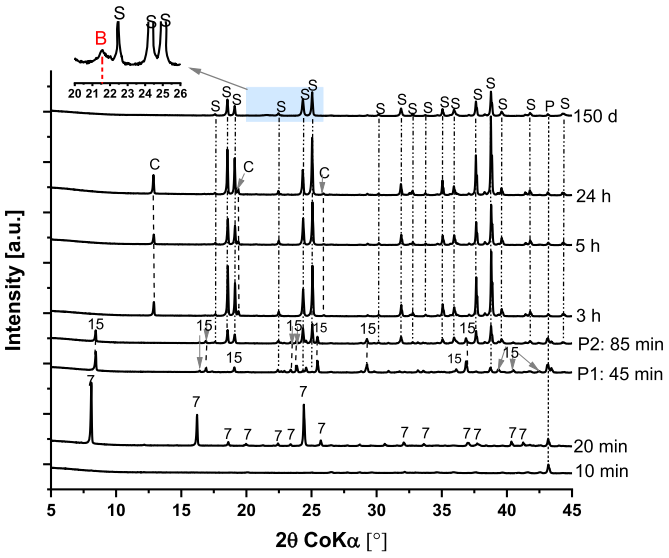

Fig. D-1. XRD patterns of the aluminum sulfate-containing suspension S4-AlS over time. 7 = phosphorrösslerite ($MgHPO_4{\cdot}7H_2O$), 15 = $Mg_2KH(PO_4)_2{\cdot}15H_2O$, B = brucite ($Mg(OH)_2$), C = cattiite ($Mg_3(PO_4)_2{\cdot}22H_2O$), P = periclase (MgO), S = K-struvite ($MgKPO_4{\cdot}6H_2O$). Note the blue highlighted pattern is further enlarged as displayed in the figure. P1 and P2 are the two characteristic points as shown in Fig. 6.

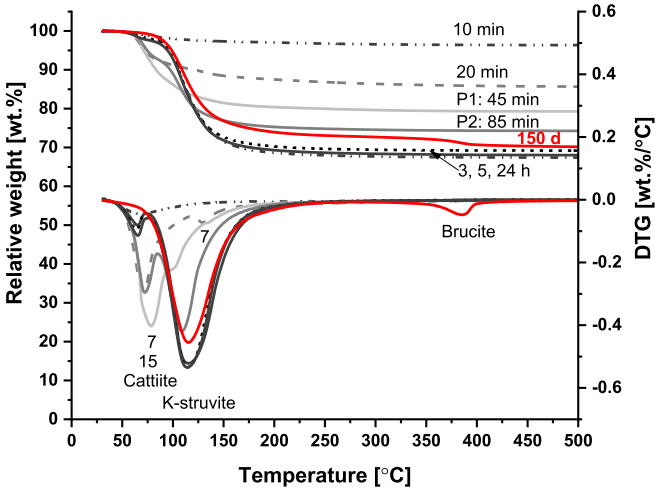

Fig. D-2. TG/DTG curves of the aluminum sulfate-containing suspension S4-AlS over time. 7 = phosphorrösslerite ($MgHPO_4{\cdot}7H_2O$), 15 = $Mg_2KH(PO_4)_2{\cdot}15H_2O$. Note P1 and P2 are the two characteristic points as shown in Fig. 6.

Appendix E

Table E
Summary of ^{31}P and ^{27}Al MAS-NMR data for magnesium-, potassium- and aluminum-containing phases from literature.

Mineral	^{31}P [δ, ppm]	^{27}Al [δ, ppm]
KH_2PO_4	3.6, 3.9 [5, 97]	–
Newberyite: $MgHPO_4{\cdot}3H_2O$	−7.5, −8 [5, 98]	–
Phosphorrösslerite: $MgHPO_4{\cdot}7H_2O$	1.7 [5]	–
Amorphous $MgHPO_4$	−2.4 [92]	
$Mg_2KH(PO_4)_2{\cdot}15H_2O$[a]	4 to 2 [5]	–
Farringtonite: $Mg_3(PO_4)_2$	−0.5 [99]	
Amorphous $Mg_3(PO_4)_2$	0.5 [99]	
Bobierrite: $Mg_3(PO_4)_2{\cdot}8H_2O$	4.6 [5, 99]	–
Cattiite[b]: $Mg_3(PO_4)_2{\cdot}22H_2O$	1.1 [99], 7.0 [5, 6]	–
K-struvite: $MgKPO_4{\cdot}6H_2O$	5.6, 6.4 [5, 18, 19, 23]	–
Amorphous aluminum hydroxide $Al(OH)_3$	–	65, 36, 8.5 [89]
Gibbsite: $Al(OH)_3$	–	8, 9.5 [89–91]
Bayerite: $Al(OH)_3$	–	11.5 [89]
Boehmite: AlOOH	–	8, 9.5 [86, 89]
Hydrotalcite: $Mg_6Al_2(OH)_{16}CO_3{\cdot}4H_2O$	–	9 [50, 88]
PO_4-LDH	10 to −10 [81] (broad signals)	11 [81]

(*continued on next page*)

Table E (*continued*)

Mineral		^{31}P [δ, ppm]	^{27}Al [δ, ppm]
Lazulite: $MgAl_{12}(OH)_2(PO_4)_2$		−20.1 [100]	*
Amorphous aluminum phosphate: $AlPO_4$		5 to −20 [94] (broad signals)	44, −5 [101] 50 to 35 [broad signals], −10 [94]
Phosphate absorbed on $Al(OH)_3$		10 to −10 [81] 0 to −20 [94] (broad signals)	8, 10 [81, 94]
Berlinite: $AlPO_4$		−25.3 [100]	*
Metavariscite: $AlPO_4{\cdot}2H_2O$		−19.3 [102]	−13.2 [102]
Variscite: $AlPO_4{\cdot}2H_2O$		−19.2 [100]	−9 [86]
$Al(H_2PO_4)_3$		−16.6 [103]	*
Augelite: $Al(OH)_3PO_4$		−29.6 [100]	*
Senegalite: $Al_2(OH)_3(PO_4){\cdot}H_2O$		−16.2 [100]	*
Wavellite: $Al_3(OH)_3(PO_4)_2{\cdot}5H_2O$		−11.2 [100]	*
$Al(HPO_4)(H_2PO_4){\cdot}3H_2O$		*	−7.6 [6, 103]
Taranakite: $K_3Al_5(HPO_4)_6(PO_4)_2{\cdot}18H_2O$		5.2, −17.2 [48]	−8.9 [6, 104]
OH-minyulite	$KAl_2(HPO_4)_2{\cdot}H_2O$	−6.5, −10.7, −12.6 [95]	*
	$KAl_2(PO_4)_2(OH){\cdot}2H_2O$ (Tinsleyite)	−6.9, −18.7 [6, 49]	*
	$KAl_2(PO_4)_2(OH){\cdot}4H_2O$	−9.6 [96]	*
	$KAl_2(PO_4)_2F{\cdot}4H_2O$	−11.2 [105]	−2.1 [105]

[a] A broad resonance was reported for synthesized $Mg_2KH(PO_4)_2{\cdot}15H_2O$, which was assumed. to be caused by the presence of amorphous materials [4].
[b] The chemical shifts of cattiite documented in [5,6,99] differ strongly, and thus more experimental data are needed for further confirmation.
* No data currently available in open literature.

Appendix F

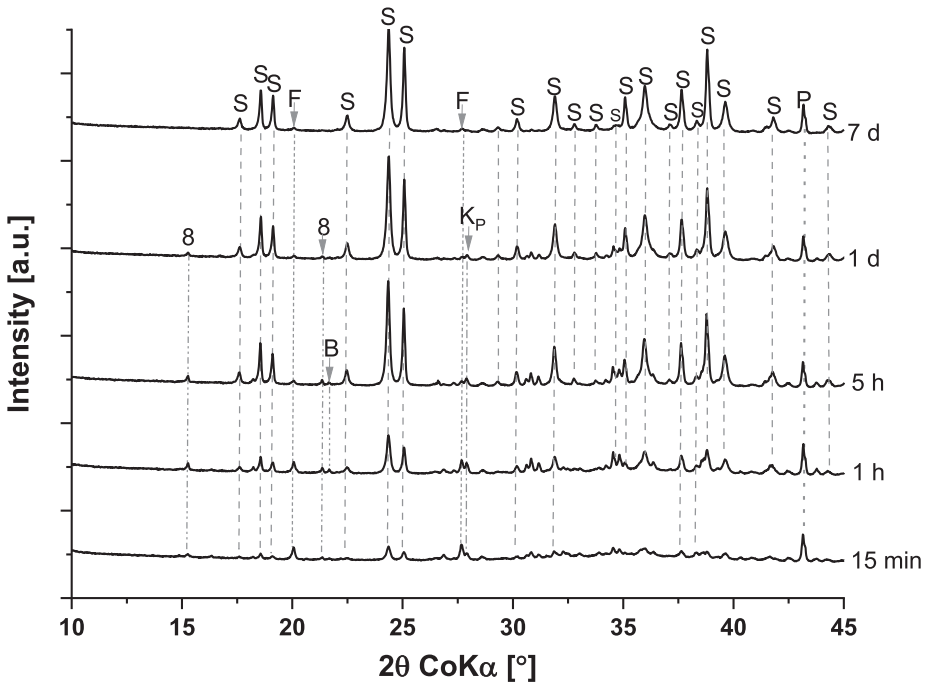

Fig. F-1. XRD patterns of the reference paste P4-R over time. 8 = bobierrite ($Mg_3(PO_4)_2{\cdot}8H_2O$), B = brucite ($Mg(OH)_2$), F = forsterite (Mg_2SiO_4), K_P = KH_2PO_4, P = periclase (MgO), S = K-struvite ($MgKPO_4{\cdot}6H_2O$).

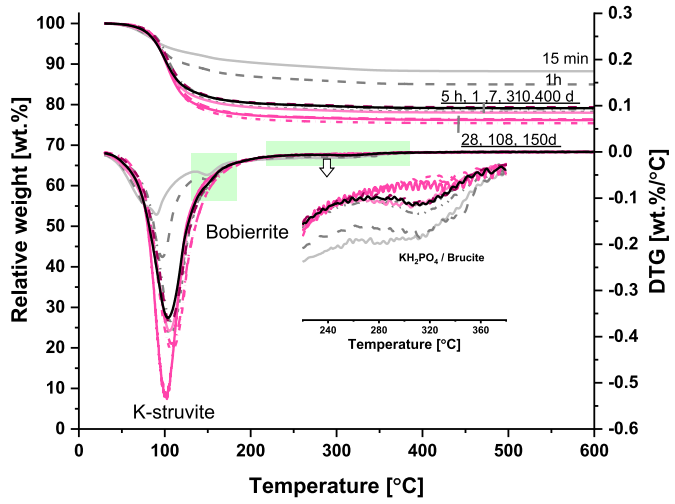

Fig. F-2. TG/DTG curves of the reference paste P4-R over time. Data after 28, 108, 150, 310 and 400 days were taken from [23].

Appendix G

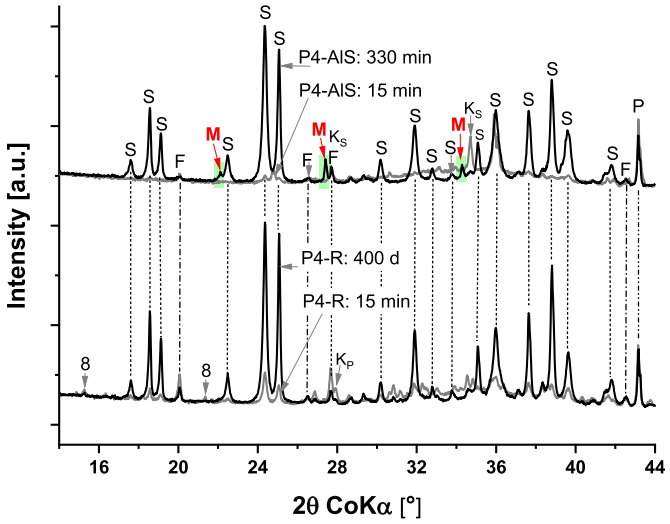

Fig. G-1. XRD patterns of the pastes without (P4-R) and with aluminum sulfate (P4-AlS) after early and late hydration. 8 = bobierrite ($Mg_3(PO_4)_2{\cdot}8H_2O$), F = forsterite (Mg_2SiO_4), K_P = KH_2PO_4, P = periclase (MgO), S = K-struvite ($MgKPO_4{\cdot}6H_2O$), M = tentatively assigned to a minyulite-like phase.

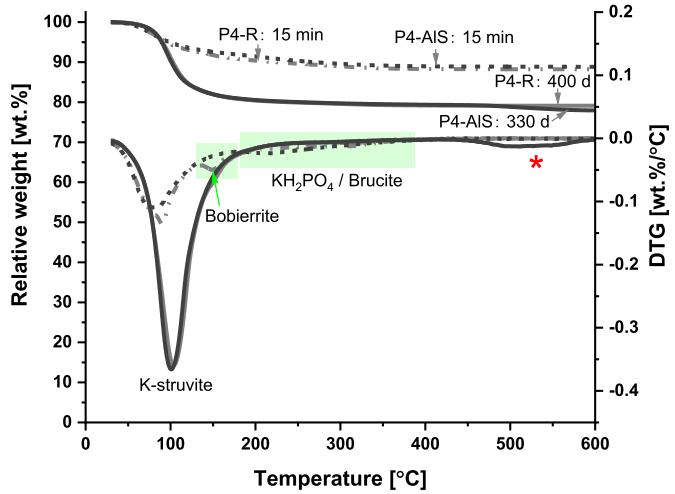

Fig. G-2. TG/DTG curves of the pastes without (P4-R) and with aluminum sulfate (P4-AlS) over time. * = unassigned weight loss.

References

[1] F. Qiao, C.K. Chau, Z. Li, Setting and strength development of magnesium phosphate cement paste, Adv. Cem. Res. 21 (2009) 175–180.
[2] B. Xu, B. Lothenbach, A. Leemann, F. Winnefeld, Reaction mechanism of magnesium potassium phosphate cement with high magnesium-to-phosphate ratio, Cem. Concr. Res. 108 (2018) 140–151.
[3] F. Qiao, C.K. Chau, Z. Li, Property evaluation of magnesium phosphate cement mortar as patch repair material, Constr. Build. Mater. 24 (2010) 695–700.
[4] H. Lahalle, C.Cau Dit Coumes, A. Mesbah, D. Lambertin, C. Cannes, S. Delpech, S. Gauffinet, Investigation of magnesium phosphate cement hydration in diluted suspension and its retardation by boric acid, Cem. Concr. Res. 87 (2016) 77–86.
[5] H. Lahalle, C.Cau Dit Coumes, C. Mercier, D. Lambertin, C. Cannes, S. Delpech, S. Gauffinet, Influence of the w/c ratio on the hydration process of a magnesium phosphate cement and on its retardation by boric acid, Cem. Concr. Res. 109 (2018) 159–174.
[6] C.Cau Dit Coumes, A. Rousselet, B. Xu, C.A. Mercier, S. Gauffinet, Investigation of aluminum nitrate as set retarder of magnesium potassium phosphate cement: mechanisms involved in diluted suspension, Cem. Concr. Res. 150 (2021) 106608.
[7] I. Buj, J. Torras, D. Casellas, M. Rovira, J. de Pablo, Effect of heavy metals and water content on the strength of magnesium phosphate cements, J. Hazard. Mater. 170 (2009) 345–350.
[8] I. Buj, J. Torras, M. Rovira, J. de Pablo, Leaching behaviour of magnesium phosphate cements containing high quantities of heavy metals, J. Hazard. Mater. 175 (2010) 789–794.
[9] J. Torras, I. Buj, M. Rovira, J. de Pablo, Semi-dynamic leaching tests of nickel containing wastes stabilized/solidified with magnesium potassium phosphate cements, J. Hazard. Mater. 186 (2011) 1954–1960.
[10] A.S. Wagh, S.Y. Sayenko, V.A. Shkuropatenko, R.V. Tarasov, M.P. Dykiy, Y. O. Svitlychniy, V.D. Virych, E.A. Ulybkina, Experimental study on cesium immobilization in struvite structures, J. Hazard. Mater. 302 (2016) 241–249.
[11] Z. Zhang, Z. Yang, Z. Chen, T. Kang, X. Ding, Y. Li, Y. Liao, C. Chen, H. Yuan, H. Peng, J. Lim, A study on bone cement containing magnesium potassium phosphate for bone repair, Cogent Biol. 4 (2018).
[12] C.Cau Dit Coumes, D. Lambertin, H. Lahalle, P. Antonucci, C. Cannes, S. Delpech, Selection of a mineral binder with potentialities for the stabilization/solidification of aluminum metal, J. Nucl. Mater. 453 (2014) 31–40.
[13] L.J. Gardner, C.L. Corkhill, S.A. Walling, J.E. Vigor, C.A. Murray, C.C. Tang, J. L. Provis, N.C. Hyatt, Early age hydration and application of blended magnesium potassium phosphate cements for reduced corrosion of reactive metals, Cem. Concr. Res. 143 (2021), 106375.
[14] S.A. Walling, J.L. Provis, Magnesia-based cements: a journey of 150 years, and cements for the future? Chem. Rev. 116 (2016) 4170–4204.
[15] M. De Campos, C.A. Davy, N. Djelal, M. Rivenet, J. Garcia, Development of a stoichiometric magnesium potassium phosphate cement (MKPC) for the immobilization of powdered minerals, Cem. Concr. Res. 142 (2021), 106346.
[16] C. Dow, F.P. Glasser, Calcium carbonate efflorescence on Portland cement and building materials, Cem. Concr. Res. 33 (2003) 147–154.
[17] M. Le Rouzic, T. Chaussadent, L. Stefan, M. Saillio, On the influence of Mg/P ratio on the properties and durability of magnesium potassium phosphate cement pastes, Cem. Concr. Res. 96 (2017) 27–41.
[18] B. Xu, F. Winnefeld, J. Kaufmann, B. Lothenbach, Influence of magnesium-to-phosphate ratio and water-to-cement ratio on hydration and properties of magnesium potassium phosphate cements, Cem. Concr. Res. 123 (2019), 105781.
[19] B. Xu, B. Lothenbach, F. Winnefeld, Influence of wollastonite on hydration and properties of magnesium potassium phosphate cements, Cem. Concr. Res. 131 (2020), 106012.
[20] B. Xu, H. Ma, H. Shao, Z. Li, B. Lothenbach, Influence of fly ash on compressive strength and micro-characteristics of magnesium potassium phosphate cement mortars, Cem. Concr. Res. 99 (2017) 86–94.
[21] D. Chartier, J. Sanchez-Canet, P. Antonucci, S. Esnouf, J.P. Renault, O. Farcy, D. Lambertin, S. Parraud, H. Lamotte, C.Cau Dit Coumes, Behaviour of magnesium phosphate cement-based materials under gamma and alpha irradiation, J. Nucl. Mater. 541 (2020) 152411.
[22] X. Liu, B. Ma, H. Tan, B. Gu, T. Zhang, P. Chen, H. Li, J. Mei, Effect of aluminum sulfate on the hydration of Portland cement, tricalcium silicate and tricalcium aluminate, Constr. Build. Mater. 232 (2020), 117179.
[23] B. Xu, F. Winnefeld, B. Lothenbach, Effect of temperature curing on properties and hydration of wollastonite blended magnesium potassium phosphate cements, Cem. Concr. Res. 142 (2021), 106370.
[24] R. Snellings, J. Chwast, Ö. Cizer, N. De Belie, Y. Dhandapani, P. Durdzinski, J. Elsen, J. Haufe, D. Hooton, C. Patapy, M. Santhanam, K. Scrivener, D. Snoeck, L. Steger, S. Tongbo, A. Vollpracht, F. Winnefeld, B. Lothenbach, RILEM TC-238 SCM recommendation on hydration stoppage by solvent exchange for the study of hydrate assemblages, Mater. Struct. 51 (2018) 172.
[25] H. Ma, B. Xu, J. Liu, H. Pei, Z. Li, Effects of water content, magnesia-to-phosphate molar ratio and age on pore structure, strength and permeability of magnesium potassium phosphate cement paste, Mater. Des. 64 (2014) 497–502.
[26] B. Xu, H. Ma, Z. Li, Influence of magnesia-to-phosphate molar ratio on microstructures, mechanical properties and thermal conductivity of magnesium potassium phosphate cement paste with large water-to-solid ratio, Cem. Concr. Res. 68 (2015) 1–9.
[27] D. Massiot, F. Fayon, M. Capron, I. King, S. Le Calvé, B. Alonso, J.O. Durand, B. Bujoli, Z. Gan, G. Hoatson, Modelling one- and two-dimensional solid-state NMR spectra, Magn. Reson. Chem. 40 (2002) 70–76.
[28] D.R. Neuville, L. Cormier, D. Massiot, Al environment in tectosilicate and peraluminous glasses: a 27Al MQ-MAS NMR, raman, and XANES investigation, Geochim. Cosmochim. Acta 68 (2004) 5071–5079.
[29] E. Bernard, B. Lothenbach, D. Rentsch, Influence of sodium nitrate on the phases formed in the MgO-Al2O3-SiO2-H2O system, Mater. Des. 198 (2021), 109391.
[30] D.A. Kulik, T. Wagner, S.V. Dmytrieva, G. Kosakowski, F.F. Hingerl, K. V. Chudnenko, U.R. Berner, in: GEM-Selektor Geochemical Modeling Package: Revised Algorithm and GEMS3K Numerical Kernel for Coupled Simulation Codes 17, 2013, pp. 1–24.
[31] T. Thoenen, W. Hummel, U. Berner, E. Curti, he PSI/Nagra Chemical Thermodynamic Database 12/07, PSI Report 14-04, Villigen PSI, Switzerland, 2014.
[32] B. Lothenbach, D.A. Kulik, T. Matschei, M. Balonis, L. Baquerizo, B. Dilnesa, G. D. Miron, R.J. Myers, Cemdata18: a chemical thermodynamic database for hydrated Portland cements and alkali-activated materials, Cem. Concr. Res. 115 (2019) 472–506.
[33] B. Lothenbach, B. Xu, F. Winnefeld, Thermodynamic data for magnesium (potassium) phosphates, Appl. Geochem. 111 (2019), 104450.
[34] L. Ciavatta, Equilibrium studies on the complexation of cations with orthophosphate ions, in: Recent Research Developments in Inorganic and Organometallic Chemistry, 2001, pp. 83–98.
[35] M. Iuliano, L. Ciavatta, G. De Tommaso, The solubility constant of variscite, Soil Sci. Soc. Am. J. 72 (2008) 343–346.
[36] P. Blanc, A. Lassin, P. Piantone, M. Azaroual, N. Jacquemet, A. Fabbri, E. C. Gaucher, Thermoddem: a geochemical database focused on low temperature water/rock interactions and waste materials, Appl. Geochem. 27 (2012) 2107–2116.
[37] D. Langmuir, Techniques of Estimating Thermodynamic Properties for Some Aqueous Complexes of Geochemical Interest, ACS Publications, 1979.
[38] W. Lindsay, P. Walthall, The solubility of aluminum in soils, in: The Environmental Chemistry of Aluminum, CRC Press, 2020, pp. 333–361.
[39] R.A. Robie, B.S. Hemingway, Thermodynamic properties of minerals and related substances at 298.15 K and 1 bar (105 Pascals) pressures and at higher temperatures, U.S. Geol. Surv. Bull. 2131 (1995) 1–461.
[40] B.P. Onac, H.S. Effenberger, Re-examination of berlinite (AlPO4) from the Cioclovina Cave, Romania, Am. Miner. 92 (2007) 1998–2001.
[41] R. Kniep, D. Mootz, A. Vegas, Variscite 33 (1977) 263–265.
[42] J.D. Bass, An Experimental Determination of the Stability and Thermochemical Properties of the Mineral Trolleite, Lehigh University, 1977.
[43] F. Capitelli, M. Saviano, M.R. Ghiara, M. Rossi, Crystal-chemical investigation of Al2(PO4)(OH)3 augelite from Rapid Creek, Yukon, Canada, Z. Kristallogr. Cryst. Mater. 229 (2014) 8–16.
[44] T.D. Keegan, T. Araki, P.B. Moore, Senegalite, Al2(OH)3(H2O)(PO4), a novel structure type, Am. Mineral. 64 (1979) 1243–1247.
[45] P. Vieillard, Y. Tardy, D. Nahon, Stability fields of clays and aluminum phosphates; parageneses in lateritic weathering of argillaceous phosphatic sediments, Am. Mineral. 64 (1979) 626–634.
[46] T. Araki, T. Zoltai, The crystal structure of wavellite, Z. Kristallogr. 127 (1968) 21–33.
[47] P.B. Moore, T. Araki, Trolleite, Al4(OH)3[PO4]3: a very dense structure with octahedral face-sharing dimers, Am. Mineral. 59 (1974) 974–984.
[48] S. Dick, U. Goβner, A. Weiβ, C. Robl, G. Groβmann, G. Ohms, T. Zeiske, Taranakite — the mineral with the longest crystallographic axis, Inorg. Chim. Acta 269 (1998) 47–57.
[49] S. Dick, G. Grossmann, G. Ohms, M. Mueller, Aluminiumphosphate mit azentrischen schicht- und raumnetzstrukturen aus topologisch verwandten motiven: 2. KAl2(PO4)2 (OH).2(H2O), Zeitschrift fuer Naturforschung B J. Chem. Sci. 52 (1997) 1447–1455.
[50] E. Bernard, W.J. Zucha, B. Lothenbach, U. Mäder, Stability of hydrotalcite (Mg-Al layered double hydroxide) in presence of different anions, Cem. Concr. Res. 152 (2022), 106674.
[51] J.R. Lehr, A.W. Frazier, J.P. Smith, A new calcium aluminum phosphate, CaAlH (PO4)2·6H2O, Soil Sci. Soc. Am. J. 28 (1964) 38–39.
[52] F. Brunet, C. Chopin, Bearthite, Ca2Al(PO4)2OH: stability, thermodynamic properties and phase relations, Contrib. Mineral. Petrol. 121 (1995) 258–266.
[53] F.B.C. Chopin, W. Gebert, O. Medenbach, E. Tillmanns, Bearthite, Ca2Al[PO4]2 (OH), a new mineral from high-pressure terranes of the western Alps, Schweiz. Mineral. Petrogr. Mitt. 73 (1993) 1–9.
[54] J.P. Owens, Z.S. Altschuler, R. Berman, Millisite in phosphorite from Homeland, Florida, Am. Mineral 45 (1960) 547–561.
[55] A.M. Blount, The crystal structure of crandallite, Am. Mineral. 59 (1974) 41–47.
[56] P.B. Moore, T. Araki, Montgomeryite, Ca4Mg(H2O)12(Al4(OH)4(PO4)6). Its crystal structure and relation to vauxite, Fe2(H2O)4 (Al4(OH)4 (H2O)4 (PO4)4) (H2O)4, Am. Mineral 59 (1974) 843–850.
[57] W. Lindsay, M. Peech, J. Clark, Solubility criteria for the existence of variscite in soils, Soil Sci. Soc. Am. J. 23 (1959) 357–360.
[58] C.V. Cole, M.L. Jackson, Solubility equilibrium constant of dihydroxy aluminum dihydrogen phosphate relating to a mechanism of phosphate fixation in soils, Soil Sci. Soc. Am. Proc. 15 (1951) 84–89.
[59] E.P. Egan Jr., Z.T. Wakefield, Low temperature heat capacity and entropy of variscite, AlPO4·2H2O, 10° to 310° K, J. Chem. Eng. Data 11 (1966) 610–611.
[60] M. Webber, Effects of temperature and time on hydroxy aluminum phosphate-montmorillonite complex, Soil Sci. 125 (1978) 107–114.
[61] A. Taylor, E. Gurney, Solubility of amorphous aluminum phosphate, Soil Sci. 93 (1962) 241–245.

[62] A. Taylor, E. Gurney, The dissolution of calcium aluminum phosphate, CaAlH(PO4)2·6H2O, Soil Sci. Soc. Am. J. 28 (1964) 63–64.
[63] W.N.De Lima, M.F. Reymao, Estudo termodinámico teórico aplicado a gênese e às alteraçòes de hidroxifosfatos naturais: Fosfatos lateriticos de Jaudìá (PA) e Pirocaua (MA) 13 (1983) 41–51.
[64] H.C. Helgeson, J.M. Delany, H.W. Nesbitt, D.K. Bird, Summary and critique of the thermodynamic properties of rock-forming minerals, Am. J. Sci. 278-A (1978) 1–229.
[65] A. Taylor, E. Gurney, Solubilities of potassium and ammonium taranakites, J. Phys. Chem. 65 (1961) 1613–1616.
[66] E.P. Egan Jr., Z.T. Wakefield, B.B. Luff, Thermodynamic properties of potassium and ammonium taranakites, J. Phys. Chem. 65 (1961) 1609–1612.
[67] A. Taylor, E. Gurney, The dissolution of basic potassium and ammonium aluminum phosphates, Soil Sci. Soc. Am. J. 28 (1964) 289–290.
[68] E.P. Egan Jr., Z.T. Wakefield, B.B. Luff, Low temperature heat capacity and entropy of basic potassium aluminum phosphate, J. Chem. Eng. Data 8 (1963) 184–185.
[69] J.O. Nriagu, Phosphate - clay mineral relations in soils and sediments, Can. J. Earth Sci. 13 (1976) 717–736.
[70] S. Kaushik, Surface Properties of Crandallite in Relation to Froth Flotation, University of British Columbia, 2012.
[71] P.H. Hsu, Crystallization of variscite at room temperature, Soil Sci. 133 (1982) 305–313.
[72] T. Roncal-Herrero, J.D. Rodríguez-Blanco, L.G. Benning, E.H. Oelkers, Precipitation of iron and aluminum phosphates directly from aqueous solution as a function of temperature from 50 to 200 °C, Cryst. Growth Des. 9 (2009) 5197–5205.
[73] K. Drüppel, A. Hösch, G. Franz, The system Al2O3-P2O5-H2O at temperatures below 200 °C: experimental data on the stability of variscite and metavariscite AlPO4·2H2O, Am. Min. 92 (2007) 1695–1703.
[74] W. Stumm, J.J. Morgan, Aquatic Chemistry. Chemical Equilibria and Rates in Natural Waters, 3rd ed., John Wiley & Sons, Inc., New York, 1996.
[75] J. Veith, G. Sposito, Reactions of aluminosilicates, aluminum hydrous oxides, and aluminum oxide with o-phosphate: the formation of X-ray amorphous analogs of variscite and montebrasite, Soil Sci. Soc. Am. J. 41 (1977) 870–876.
[76] Y.S. Chen, J.N. Butler, W. Stumm, Kinetic study of phosphate reaction with aluminum oxide and kaolinite, Environ. Sci. Technol. 7 (1973) 327–332.
[77] T.J. Van Emmerik, D.E. Sandström, O.N. Antzutkin, M.J. Angove, B.B. Johnson, 31P solid-state nuclear magnetic resonance study of the sorption of phosphate onto gibbsite and kaolinite, Langmuir 23 (2007) 3205–3213.
[78] W. Wise, S. Loh, Equilibria and origin of minerals in the system Al2O3-AlPO4-H2O, Am Min 61 (1976) 409–413.
[79] S. Dick, The structure of synthetic Tinsleyite KA12(PO4)2(OH).2H2O, Z Naturforsch 54 (b) (1999) 1385–1390.
[80] G.P. Gillman, M.A. Noble, M.D. Raven, Anion substitution of nitrate-saturated layered double hydroxide of mg and Al, Appl. Clay Sci. 38 (2008) 179–186.
[81] C. Liu, M. Zhang, G. Pan, L. Lundehøj, U.G. Nielsen, Y. Shi, H.C.B. Hansen, Phosphate capture by ultrathin MgAl layered double hydroxide nanoparticles, Appl. Clay Sci. 177 (2019) 82–90.
[82] P. Karkanas, O. Bar-Yosef, P. Goldberg, S. Weiner, Diagenesis in prehistoric caves: the use of minerals that form in situ to assess the completeness of the archaeological record, J. Archaeol. Sci. 27 (2000) 915–929.
[83] J.O. Nriagu, Phosphate – clay mineral relations in soils and sediments, Can. J. Earth Sci. 13 (1976) 717–736.
[84] P.B. Moore, A.R. Kampf, T. Araki, Foggite, (CaH2O)2 (CaAl2 (OH)4 (PO4)2): its atomic arrangement and relationship to calcium Tschermak's pyroxene, Am. Mineral. 60 (1975) 965–971.
[85] R. Boistelle, F. Abbona, H.E. Lundager Madsen, On the transformation of struvite into newberyite in aqueous systems, Phys. Chem. Minerals 9 (1983) 216–222.
[86] J. Klein, M. Ushio, L.S. Burrell, B. Wenslow, S.L. Hem, Analysis of aluminum hydroxyphosphate vaccine adjuvants by 27Al MAS NMR, J. Pharm. Sci. 89 (2000) 311–321.
[87] R. Lookman, P. Grobet, R. Merckx, K. Vlassak, Phosphate sorption by synthetic amorphous aluminium hydroxides: a 27Al and 31P solid-state MAS NMR spectroscopy study, Eur. J. Soil Sci. 45 (1994) 37–44.
[88] K.J.D. MacKenzie, R.H. Meinhold, B.L. Sherriff, Z. Xu, 27Al and 25Mg solid-state magic-angle spinning nuclear magnetic resonance study of hydrotalcite and its thermal decomposition sequence, J. Mater. Chem. 3 (1993) 1263–1269.
[89] T. Isobe, T. Watanabe, J.B. d'Espinose de la Caillerie, A.P. Legrand, D. Massiot, Solid-state 1H and 27Al NMR studies of amorphous aluminum hydroxides, J. Colloid Interface Sci. 261 (2003) 320–324.
[90] A.C. Kunwar, A.R. Thompson, H.S. Gutowsky, E. Oldfield, Solid state aluminum-27 NMR studies of tridecameric Al-OxoHydroxy clusters in basic aluminum selenate, sulfate, and the mineral zunyite, J. Magn. Reson. 60 (1984) 467–472.
[91] S.J. Duffy, G.W. VanLoon, Investigations of aluminum hydroxyphosphates and activated sludge by 27Al and 31P MAS NMR, Can. J. Chem. 73 (1995) 1645–1659.
[92] V. Borau, C. Jiménez, J.M. Marinas, F.J. Romero, J.R. Ruiz, M.A. Aramendía, Characterization by XRD, DRIFT, and MAS NMR spectroscopies of a Mg2P2O7 catalyst, J. Colloid Interface Sci. 202 (1998) 456–461.
[93] S.N. Scrimgeour, J.A. Chudek, G.A. Cowper, C.H. Lloyd, 31P solid-state MAS-NMR spectroscopy of the compounds that form in phosphate-bonded dental casting investment materials during setting, Dent. Mater. 23 (2007) 934–943.
[94] R. Lookman, P. Grobet, R. Merckx, W.H. Van Riemsdijk, Application of 31P and 27Al MAS NMR for phosphate speciation studies in soil and aluminium hydroxides: promises and constraints, Geoderma 80 (1997) 369–388.
[95] S. Dick, U. Goßner, A. Weiss, C. Robl, G. Grossmann, G. Ohms, M. Müller, The potassium aluminum phosphate KAl(HPO4)2·H2O: X-ray diffraction, neutron-scattering, and solid-state NMR characterization, J. Solid State Chem. 132 (1997) 47–55.
[96] S. Dick, G. Grossmann, G. Ohms, T. Zeiske, Aluminum phosphates with non-centrosymmetric layer- and framework-structures of topologically related motifs. Part 1. KAl2(PO4)2(OH)·4H2O, Zeitschrift fuer Naturforschung Sect. B J. Chem. Sci. 52 (1997) 1439–1446.
[97] L.J. Gardner, S.A. Bernal, S.A. Walling, C.L. Corkhill, J.L. Provis, N.C. Hyatt, Characterisation of magnesium potassium phosphate cements blended with fly ash and ground granulated blast furnace slag, Cem. Concr. Res. 74 (2015) 78–87.
[98] S.N. Scrimgeour, J.A. Chudek, C.H. Lloyd, The determination of phosphorus containing compounds in dental casting investment products by 31P solid-state MAS-NMR spectroscopy, Dent. Mater. 23 (2007) 415–424.
[99] V. Borau, C. Jiménez, J.M. Marinas, F.J. Romero, J.R. Ruiz, M.A. Aramendía, XRD and solid-state NMR study of magnesium oxide–magnesium orthophosphate systems, J. Solid State Chem. 135 (1998) 96–102.
[100] W.F. Bleam, P.E. Pfeffer, J.S. Frye, 31P solid-state nuclear magnetic resonance spectroscopy of aluminum phosphate minerals, Phys. Chem. Miner. 16 (1989) 455–464.
[101] L. Lundehøj, H.C. Jensen, L. Wybrandt, U.G. Nielsen, M.L. Christensen, C.A. Quist-Jensen, Layered double hydroxides for phosphorus recovery from acidified and non-acidified dewatered sludge, Water Res. 153 (2019) 208–216.
[102] C.S. Blackwell, R.L. Patton, Aluminum-27 and phosphorus-31 nuclear magnetic resonance studies of aluminophosphate molecular sieves, J. Phys. Chem. 88 (1984) 6135–6139.
[103] D. Müller, I. Grunze, E. Hallas, G. Ladwig, Hochfeld-27Al-NMR-untersuchungen zur aluminiumkoordination in kristallinen aluminiumphosphaten, Z. Anorg. Allg. Chem. 500 (1983) 80–88.
[104] W.F. Bleam, P.E. Pfeffer, J.S. Frye, 31P and 27Al solid-state nuclear magnetic resonance study of taranakite, Phys. Chem. Miner. 16 (1989) 809–816.